Materials & Design 207 (2021) 109842

Contents lists available at ScienceDirect

Materials & Design

journal homepage: www.elsevier.com/locate/matdes

Physics-guided multi-objective mixture optimization for functional cementitious composites containing microencapsulated phase changing materials

Zhenglai Shen [a], Adam L Brooks [a], Yawen He [a], Jialai Wang [b], Hongyu Zhou [a,*]

[a] Civil and Environmental Engineering, University of Tennessee, Knoxville, TN 37996, United States
[b] Civil, Construction, and Environmental Engineering, University of Alabama, Tuscaloosa, AL 35294, United States

HIGHLIGHTS

- A physics-guided optimization procedure is developed for the mixture design of functional cementitious composites.
- Physics-based models are used to elucidate the composition-structure–property correlations.
- A multi-attribute decision-making process is developed to account for competing performance and cost indices.

GRAPHICAL ABSTRACT

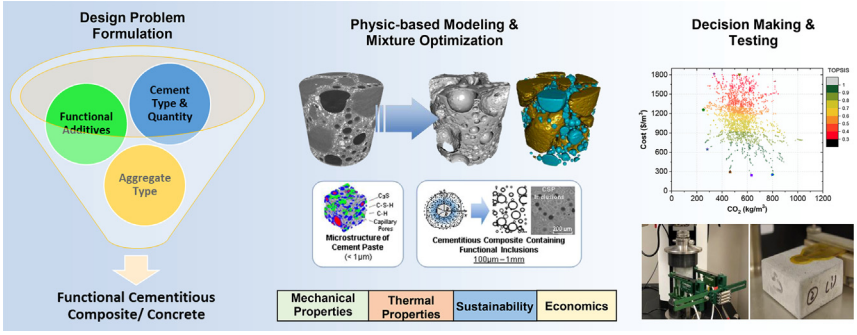

ARTICLE INFO

Article history:
Received 30 December 2020
Revised 2 May 2021
Accepted 18 May 2021
Available online 19 May 2021

Keywords:
Mixture design
Optimization
Cementitious composites
Microencapsulated phase change material (MEPCM)

ABSTRACT

A physics-guided multi-objective optimization procedure is developed for the mixture design of functional cementitious materials containing microencapsulated phase change materials (MEPCM). The mixture design procedure combines physics-based models with multi-objective optimization and decision-making methods to meet user's demands on material's mechanical and thermal properties, as well as the requirements for sustainability, functionalities, and cost. Physics-based models were utilized to draw the linkage between design variables and objective functions, including a hydration model to capture the hydration kinetics of slag-blended cement and a multiscale sub-stepping homogenization model to obtain the properties of cementitious composite. The multi-objective feasible enhanced particle swarm optimization (MOFEPSO) algorithm and the technique for preference by similarity to an ideal solution (TOPSIS) algorithm are used for mixture optimization and decision-making. The material design method is demonstrated through the design of functional cementitious composite materials containing two MEPCMs – i.e., a polymer encapsulated paraffin wax (PolyPCM) and a recently developed fly-ash cenosphere encapsulated PCM (CenoPCM). The design decision-making charts show the trade-offs among mechanical, thermal, and economic performances of cementitious composites containing MEPCMs. The mixture optimization and decision-making method can be used to assist the design of a variety types of functional cementitious composite and concrete.

* Corresponding author at: 851 Neyland Drive, 325 John D. Tickle Building, Knoxville, TN 37996-2313, United States.
E-mail address: hzhou8@utk.edu (H. Zhou).

https://doi.org/10.1016/j.matdes.2021.109842
0264-1275/

Nomenclature

A_1, A_2, A_3	Coefficients of the core–shell material elastic properties [-]
a_{ij}	Loosing effect coefficient [-]
B	Global optimal set
B_1, B_2,	Rate of the initial shell formation and decay [cm/h]
B_{sg}	Reaction coefficient [-]
b_{ij}	Wall effect coefficient [-]
C	Elastic tensor
C_1, C_2	Social (global) and cognitive (personal) acceleration coefficient [-]
CC^+	The closeness coefficient [-]
Cost	Cost [USD]
CO_2	Carbon footprint [kg]
CW_{free}	Amount of capillary water at the exterior of hydration products [kg]
D_e	Initial diffusion coefficient of water [-]
D	Personal optimal set
d	Particle size [-]
E	Elastic modulus [GPa]
f	Functional relationship
H	Exponent coefficient to calculate the amount of capillary free water [-]
h	The h^{th} constituents in functional cementitious composites
G	Shear modulus [GPa]
K	Bulk modulus [GPa]
L	Latent heat of fusion [kJ/kg]
l_c	Characteristic length of cubical representative volume element (RVE)
m	Mass [kg]
MCDM	Multi-criteria decision-making
MPD	Maximum packing density
n	classes of particle sizes
PSD	particle size distribution
p	Position vector in MOFEPSO
p	Position of feasible or non-feasible particle
p^{Λ}, p^{Ω}	Randomly selected global and personal best
$q_{s,c}$, $q_{s,sg}$	weight fraction of SiO_2 in cement and slag [-]
RCH_{CE}	Mass of CH produced from unit mass of cement hydration [kg]
r	Radius
r_0	Average radius of cement particle [um]
r_1, r_2	Inner and outer radius of a core–shell particle [um]
r_{ITZ}	Thickness of interface transition zone [um]
r_{sg0}	Radius of the slag particle [um]
rr_{sg}	Slag replacement ratio [-]
S	Specific surface area of cement [m^2]
$\mathbf{S}_m^{\mathrm{C}}$	Eshelby's tensor
S_w	Effective contact area between the surrounding capillary water and cement particles [m^2]
S_0	Total area when cement hydration products progress unconstrained [m^2]
T	Temperature [K]
t	Time [second]
v	Velocity vector
v	Velocity of feasible or non-feasible particle
VHF	Volumetric heat of fusion [J/Km^3]
w	weight
w/c	Water to cementitious binder ratio [-]
w_g	Physically bound water in hydration products [kg]
X	Elastic and thermal properties
x	Vector of mixture design variables
y_i	Ratio of i^{th} class particle volume fraction to the overall particle volume fraction [-]
z_1, z_2	Uniform distributed random numbers

Greek symbols

α	Degree of hydration
β	Residual packing density
γ	Virtual packing density
δ	Volumetric ratio of the core in a core–shell particle
ε	Weighted and normalized objective value
ε^+, ε^-	Position, negative ideal point
ζ	Compaction index
κ	Objective values
$\mu_{1\text{-}4}$	Temperature sensitivity coefficients
ν	Poisson's ratio [-]
Ξ	Sensitivity coefficient
ξ	Inertia factor
ρ	Density [kg/m^3]
σ^+, σ^-	Distance from position, negative ideal point
Γ	Concentration factor
$\mathbf{\Gamma}$	Normalized objective value [-]
υ_c	Stoichiometric ratio of mass of water to mass of cement [-]
υ_{sg}	stoichiometric ratio of the mass of CH to slag
ϕ	Volume fraction [-]
χ	Thermal conductivity [W/mK]
ψ	Power exponent of interface transition zone property [-]
ω_d	Effective diffusion coefficient of capillary water through C-S-H gel
ω_{rk}	Reaction coefficient of the boundary reaction process for the k^{th} clinker
ω_{rsg}	Reaction coefficient of slag

Subscripts and superscripts

CH	Calcium hydroxide
C-S-H	Calcium silicate hydrate
c	Cement
cap	Capillary water
cbm	Chemically bound water
core	Core
eff	Effective property
eq	Equivalent property
I	Inclusion
i	i^{th} class particle
ITZ	Interface transition zone
j	j^{th} class particle
k	k^{th} clinker of cement
MT	Mori-Tanaka model
m	Matrix
min	Minimum
o, O	The o^{th} point, and total point in the optimal set
other	Other hydration products
pcm	Phase change material
s	Sand particle
shell	Shell of core–shell particle
sg	Slag
u, U	The *u*th criteria, and total criteria of the MCDM problem
unhy	Unhydrated cement-slag blends
w	Water
Λ	Global best
Ω	Personal best
η	Decision variable
τ	The τ^{th} feasible particle

1. Introduction

The incorporation of phase change material (PCM) into cementitious composites is an effective means to enhance the thermal energy storage of concrete and thus is useful for thermally regulated energy efficient building applications. Microencapsulate phase change materials (MEPCMs) as functional fillers can be easily incorporated into materials that are commonly used in building construction while effectively avoiding PCM leaking and increasing the interface areas between PCM and host matrix [1]. Previous research on functional cementitious composites containing MEPCMs mainly focuses on its energy saving potentials and very few researches studied the approach for optimal mixture design [2]. An optimal mixture design of cementitious composites containing MEPCMs should not only meet the strength and workability requirements, but also satisfy the requirements for economy, sustainability, while possessing desired properties like high elastic modulus, high thermal conductivity and sufficient heat storage capacity. However, there often exists competing objectives which conflict with one another – for example, high volumetric heat of fusion is normally achieved through increasing the volumetric loading of the functional additives (e.g., MEPCMs), which usually leads to impaired mechanical performances and increased material cost. Therefore, it is necessary to consider the tradeoffs between the competing objectives to balance these desired functionalities in the process of the mixture design.

Concrete mixture design, also known as mixture proportioning, is the process of selecting the type and quantity of individual constituents to yield properties to meet specifications for a particular application. In general, two main approaches have been used for design concrete mixtures: prescriptive and performance-based. Prescriptive approaches are step-by-step design methodologies that specify the type and quantity of each constituents of concrete; whereas performance-based mixture design methodologies impose no strict guidelines on the amounts and ratios of constituents. Rather, this approach grants the designer substantial degrees of freedom to meet design specifications through, e.g., laboratory trial batches. Given the flexibility of performance-based approaches and a desire to satisfy multiple design objectives rather than focusing only on strength and cost, many research studies have attempted experimental optimization of concrete mixtures. For example, De Larrad and Sedran [3] proposed a solid suspension model to optimize the packing density of cementitious material which leads to very high compressive strength (236 MPa at 4-day age). Xie et al. [4] used slump, compressive strength, and durability to select optimum mix parameters of self-compacting concrete with ultra-pulverized fly ash. Soudki et al. [5] applied full factorial experiment design to maximize the compressive strength of concrete mixture by varying the water to cement ratio, coarse aggregate to total aggregate ratio, total aggregate to cement ratio, and curing time. To reducing trial batches, experimental design methods such as Taguchi method [6–8], simplex centroid design method [9,10] and Box-Behnken design of response surface methodology [11,12] are commonly used in experimental based optimization.

While experimental-based optimization methods provides powerful and useful pathways to design concrete mixtures that achieve certain design objectives, these methods are questioned since they typically require a lengthy and iterative experimental process and may not lead to truly best-performance solutions [13]. Therefore, computational-based optimization methods have been increasingly investigated to circumvent the limitations of experimental-based optimization approaches. Computational design optimization of concrete mixtures is a mathematical, as opposed to experimental, approach to mixture proportioning. In computational design optimization, the problem formulation involves defining the decision variables, objectives, and constraints of the problem. Physics-based, statistical, or machine learning models are developed to define mathematical relationships that link each objective as a function of the decision variable. Machine learning methods, such as neural network, random forest, and support vector machine, have been applied in the optimal mixture design of normal strength concrete [14,15], high strength concrete [16,17], and silica fume concrete [18]. While machine learning models have shown great potential in concrete mixture design, like statistical models, they generally depend on the availability of large experimental datasets to train and test models. For functional cementitious composites such as the ones containing microencapsulated phase change materials (MEPCMs), there still lacks datasets to establish meaningful machine learning models. As an alternative, physics-based models can be applied to establish such relationships between mixture design variables and desired properties, i.e., thermal and mechanical properties as well as economic and environmental performance indices.

This paper presents a physics-guided multi-objective optimization procedure to support the mixture design of functional cementitious composites such as those containing PCM microcapsules for thermal energy storage, see Fig. 1. The mixture design procedure combines physics-based models with a multi-objective optimization algorithm and multi-criteria decision making (MCDM) models to aid the mixture design decision-making. First, the linkage between decision variables (e.g., volume loading of different constituents, w/c, and dosage of the functional additives) and the design objectives (i.e., mechanical, thermal properties, as well as cost and sustainability indices) together with some constraints are modeled through physic-based models. The multi-objective feasible enhanced particle swarm optimization (MOFEPSO) algorithm [19] is applied to obtain the optimal set of mixture designs that are not dominated by one another. Then, a multi-criteria decision-making (MCDM) model – e.g., the technique for preference by similarity to an ideal solution (TOPSIS) algorithm, is applied to decide candidate mixture designs based on different design scenarios (i.e., mechanical properties, thermal properties, CO_2 footprint, and cost). Lastly, trial batch tests are performed to evaluate the candidate mixture design solutions and determine the final mixture.

2. Multi-objective optimization of functional cementitious composite materials

2.1. Formulation of the optimization problem

2.1.1. Decision variable and objective functions

The optimal mixture design of cementitious composites is often dictated by functional requirements and user demand. For cementitious composites containing microencapsulated PCM materials aiming to have thermal energy storage functions, high volumetric heat of fusion (i.e., heat storage capacity), high thermal conductivity, high mechanical properties (elastic modulus and compressive strength), and low CO_2 footprint and material cost are generally desired [2].

The mixture design variables considered in this study include water to cementitious binder ratio (w/c), slag replacement ratio (rr_{sg}) as a representation of using supplementary cementitious materials (SCMs) to achieve sustainability goals, and the volume fractions of the cement binder matrix (ϕ_m), aggregates (ϕ_s), and MEPCM additives (ϕ_{pcm}).

The objectives can be express in their function forms as:

$$f_1 = \text{maximize}(VHF_{eff})\ f_{VHF}\left(\phi_{pcm}, \rho_{pcm}, L_{pcm}\right) \quad (1)$$

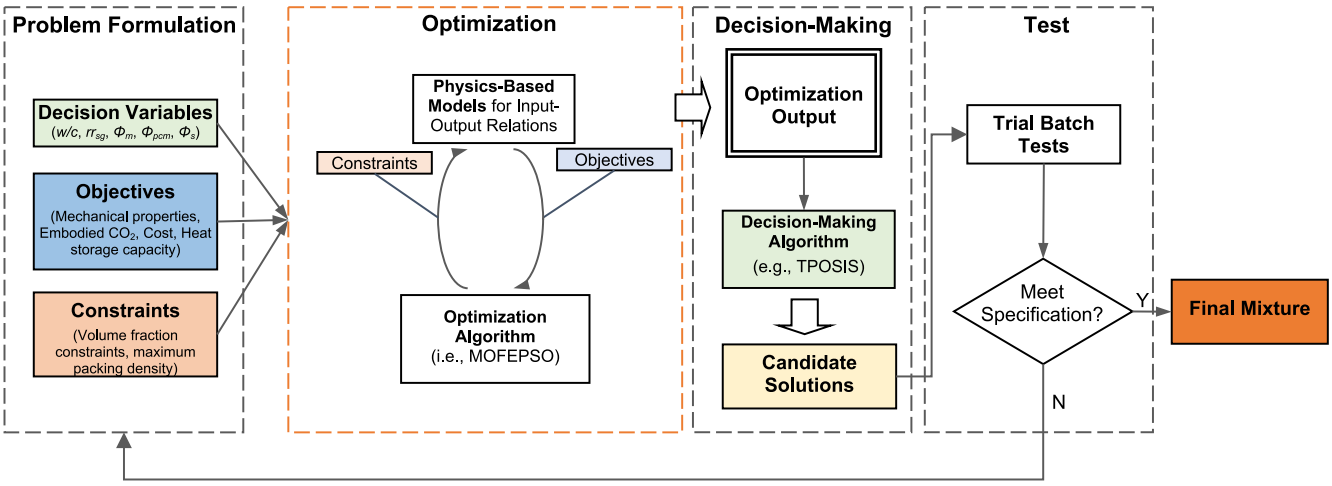

Fig. 1. Conceptual diagram showing the physics guided multi-objective optimization procedure for mixture design of cementitious composites containing MEPCMs.

$$f_2 = \text{maximize}\left(\chi_{eff}\right) f_\chi\left(\chi_m\left(w/c, rr_{sg}, t, T\right), \chi_{pcm}^{eq}, \chi_s, \phi_m, \phi_{pcm}, \phi_s, PSD\right) \tag{2}$$

$$f_3 = \text{maximize}\left(E_{eff}\right) f_E\Big(G_m\left(w/c, rr_{sg}, t, T\right), G_{pcm}^{eq}, G_s, K_m\left(w/c, rr_{sg}, t, T\right), K_{pcm}^{eq}, K_s, \phi_m, \phi_{pcm}, \phi_s, PSD\Big) \tag{3}$$

$$f_4 = \text{minimize}(CO_2)\, f_{CO_2}\left(CO_{2-m}\left(w/c, rr_{sg}\right), CO_{2-pcm}, CO_{2-s}, \phi_m, \phi_{pcm}, \phi_s\right) \tag{4}$$

$$f_5 = \text{minimize}(Cost)\, f_{\text{Cost}}\left(Cost_m\left(w/c, rr_{sg}\right), Cost_{pcm}, Cost_s, \phi_m, \phi_{pcm}, \phi_s\right) \tag{5}$$

where f_1 is the objective function for volumetric heat capacity (VHF), which is expressed as a function of the volume fraction (ϕ_{pcm}), density (ρ_{pcm}), and latent heat of PCM (L_{pcm}). For cementitious composites designed for heat storage purpose, high volumetric heat of fusion is desired. f_2 and f_3 represent the objective functions of thermal conductivity (χ) and elastic modulus (E), respectively. Higher thermal conductivity and larger elastic modulus are often desired since higher thermal conductivity helps to effectively store/release heat from phase change materials while higher elastic modulus ensures the material's mechanical performance. f_2 and f_3 are the functions of the volume fractions of each constituents (ϕ_m, ϕ_{pcm}, ϕ_s), their size distributions, as well as the properties of the constituents. In this research, ground granulated blast furnace slag (abbreviated as slag) is considered as an example of the supplementary cement material (SCM). The matrix properties (χ_m, G_m and K_m) can be expressed as the function of mixture design variables w/c, rr_{sg}, t(curing time), and T (curing temperature) using physics-based models. It is noted that compressive strength was not directly modeled in this study, alternatively, compressive strength was estimated from its relationship with density and elastic modulus given by ACI 318 [20]. Lastly, f_4 and f_5 are the objective functions for the material's carbon footprint (CO_2) and cost. Lower carbon footprint (sustainability) and low cost (economic) are desired in material design.

2.1.2. Constraints

For cementitious composite materials containing functional additives such as microencapsulated PCM, the volumetric concentration of PCM materials is typically under 0.3 according to the review work of Drissi et al. [2]. The slag replacement ratio (rr_{sg}) in this study is selected between 0 and 0.5 – i.e., the optimum slag replacement ratio is typically less than 0.5 [21] since higher slag ratio may retard the hydration. The water/cement ratio is assumed to be between 0.3 and 0.5 to ensure a balanced strength and workability, In addition, the inclusion phases in cement mortar/ concrete (aggregates, and the functional fillers) need to satisfy the maximum packing density (MPD) requirement [22], which is described using the compressible packing density model. Therefore, the following constraints are applied to the optimization problem:

$$0.3 \leqslant w/c \leqslant 0.5 \tag{6}$$

$$0 \leqslant rr_{sg} \leqslant 0.5 \tag{7}$$

$$0 \leqslant \phi_m \leqslant 1 \tag{8}$$

$$0 \leqslant \phi_{pcm} \leqslant 0.3 \tag{9}$$

$$\phi_m + \phi_{pcm} + \phi_s = 1 \tag{10}$$

$$\phi_{pcm} + \phi_s \leqslant f_{MPD}\left(PSD, \phi_{pcm}, \phi_s\right) \tag{11}$$

As shown in Eq. (11), the total volume fraction of the particulate inclusion phases, i.e., aggregates and functional fillers, cannot exceed the limit of corresponding maximum packing density, which is calculated using the compressible packing model in this study [22]. For polydispersed particles (the inclusion phases are assumed to be represented by spherical particles), we assume that the particles can be classified into n classes with particle sizes $d_1 \geqslant \cdots \geqslant d_i \geqslant \cdots \geqslant d_n$, and ϕ_i is the volume fraction of the i^{th} class particle. When the i^{th} class particle is dominant, the virtual packing density γ_i, which is defined as the maximum packing density achievable for a given mixture with each particle keeping its original shape, can be calculated as [22] :

$$\gamma_i = \frac{\beta_i}{1 - \sum_{j=1}^{i-1}\left[1 - \beta_i + b_{ij}\beta_i\left(1 - 1/\beta_j\right)\right]y_j - \sum_{j=i+1}^{n}\left[1 - a_{ij}\beta_i/\beta_j\right]y_j} \tag{12}$$

where β_i is the residual packing density of the i^{th} class particle, $y_i = \phi_i/\phi$ with $\phi = \sum_{i=1}^{n}\phi_i$; a_{ij} and b_{ij} are the loosing effect coefficient and wall effect coefficient (see Fig. 2) and

$$a_{ij} = \sqrt{1 - \left(1 - d_j/d_i\right)^{1.02}} \tag{13-1}$$

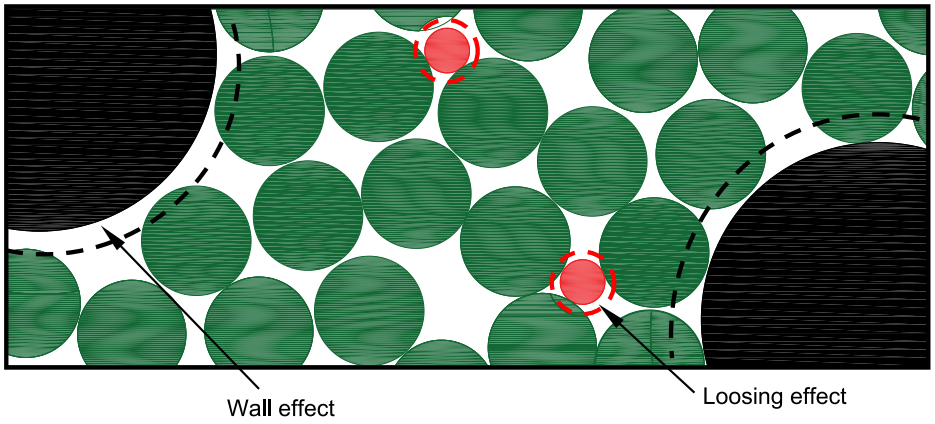

Fig. 2. Wall effect and loosing effect for a polydispersed inclusion mix.

$$b_{ij} = 1 - \left(1 - d_i/d_j\right)^{1.50} \tag{13-2}$$

Then, the actual packing density is deduced from the virtual packing density by introducing a compaction index ζ, which can be expressed as::

$$\zeta = \sum_{i=1}^{n} \zeta_i = \sum_{i=1}^{n} \frac{y_i/\beta_i}{1/\phi - 1/\gamma_i} \tag{14}$$

The compaction index is a characteristic of the packing process and it is a strictly increasing function of ϕ. The characteristic value of the compaction index is selected to be 9.0 in this study, which represents both vibration and compaction of the particle mixture [23]. In this study, silica sand and microencapsulated PCMs – i.e., both a polymer encapsulated paraffin PCM (or PolyPCM) and fly-ash cenosphere encapsulated fatty-acid (or CenoPCM), are assumed to be a random mix and have the residual packing densities of 0.64, 0.60, and 0.60, respectively, as suggested by [22].

2.2. Physics-based modeling to link the design variables and objectives

2.2.1. Multistep sub-stepping homogenization

The thermal and mechanical properties of functional cementitious composites and concretes is largely governed by their hierarchical microstructure [24]. At the cement paste level, both unreacted materials (e.g., cement clinkers and slag) and hydration products are present. The properties of hardened cement paste are dictated by the relative amount and distribution of C-S-H and inclusions of anhydrous, portlandite, ettringite, and capillary pores [25]. For cementitious composites containing functional inclusions, a single functional particle is typically comprised of a functional core (i.e., PCM) and an outer shell. Since most shells are not reactive to cement, an interfacial transition zone (ITZ) is developed between the surface of functional inclusions and the cement matrix [26]. At mesoscale (i.e., dimension from a few hundred microns to millimeters range), entrapped air bubbles, fine and coarse aggregates are incorporated as if the cementitious matrix containing micro-size functional particles is a homogenized medium [24].

Fig. 3 presents the hierarchical microstructure of cementitious composite materials. Base on it, the multi-step sub-stepping homogenization modelling scheme [27] was developed and it was used in this study for predicting the properties of cementitious composites containing MEPCM inclusions. First, the effective elastic modulus of cement paste is calculated using the Mori-Tanaka model [28], where both the hydration products in cement paste, unhydrated clinkers and slag particles, and capillary pores, that coexist in cement paste are considered. Then, the inclusion phases including MEPCM particles and aggregates (i.e., sand and gravels) are homogenized into the cement paste, where the effective property of the MEPCM particles is obtained by the equivalence model developed by the authors [27]. The interfacial transition zone (or ITZ) between the inclusion phases and cement paste is modelled using a differential homogenization method [27]. The multi-step sub-stepping homogenization model assumes that the problem contains two or more scales which are well separated – i.e., the microscopic scale (microstructure of cement paste) is small enough for the heterogeneities to be smeared out in the next scale level computation.

2.2.2. Hydration and microstructure development of slag-blended cement

Fig. 4 presents the schematic hydration process of slag-blended cement, where three sub-processes take place, i.e., cement hydration, slag hydration, and the inter-reaction between cement and slag. When water is added in the Portland cement and slag mixture, Portland cement starts to hydrate immediately. Meanwhile, a small amount of slag reacts due to the presence of gypsum. Then, the hydration of slag is activated by alkalis and the Portlandite (CH) produced in the process of cement hydration. In this research, the slag-blended cement hydration model developed by Han-seung and Wang is adopted [29]. The model was originally proposed by Tomosawa [30] and advanced by Park et al. [31]. In this microstructural model, the cement/slag particles are assumed to be spherical, uniformly sized, and uniformly distributed throughout the slag blended cement, where the hydration products grows uniformly at the surface of the particle and therefore the overall shape remains spherical over the hydration process, see Fig. 4. The cement hydration is formulated in a cubical representative volume element (RVE) with characteristic length $l_c = \sqrt[3]{4\pi(\rho_c w/c + 1)/3}r_0$, where $r_0 = 3/S\rho_c$ is the average radius of a cement particle where S is the specific surface area of cement and ρ_c is the density of cement. The RVE characteristic length of slag (l_{sg}) can be calculated similarly.

The hydration of cement and slag is comprised of the processes of nucleation, diffusion, and formation of hydration shell of cement. The cement hydration model is expressed as [29]:

$$\frac{d\alpha_k}{dt} = \frac{3(S_w/S_0)\rho_w C W_{free}}{(\upsilon_c + w_g) r_0 \rho_c} \times \frac{1}{\left(\frac{1}{\omega_{dc}} - \frac{r_0}{D_{ec}}\right) + \frac{r_0}{D_{ec}}(1-\alpha_k)^{(-1/3)} + \frac{1}{\omega_{rk}}(1-\alpha_k)^{(-2/3)}} \tag{15}$$

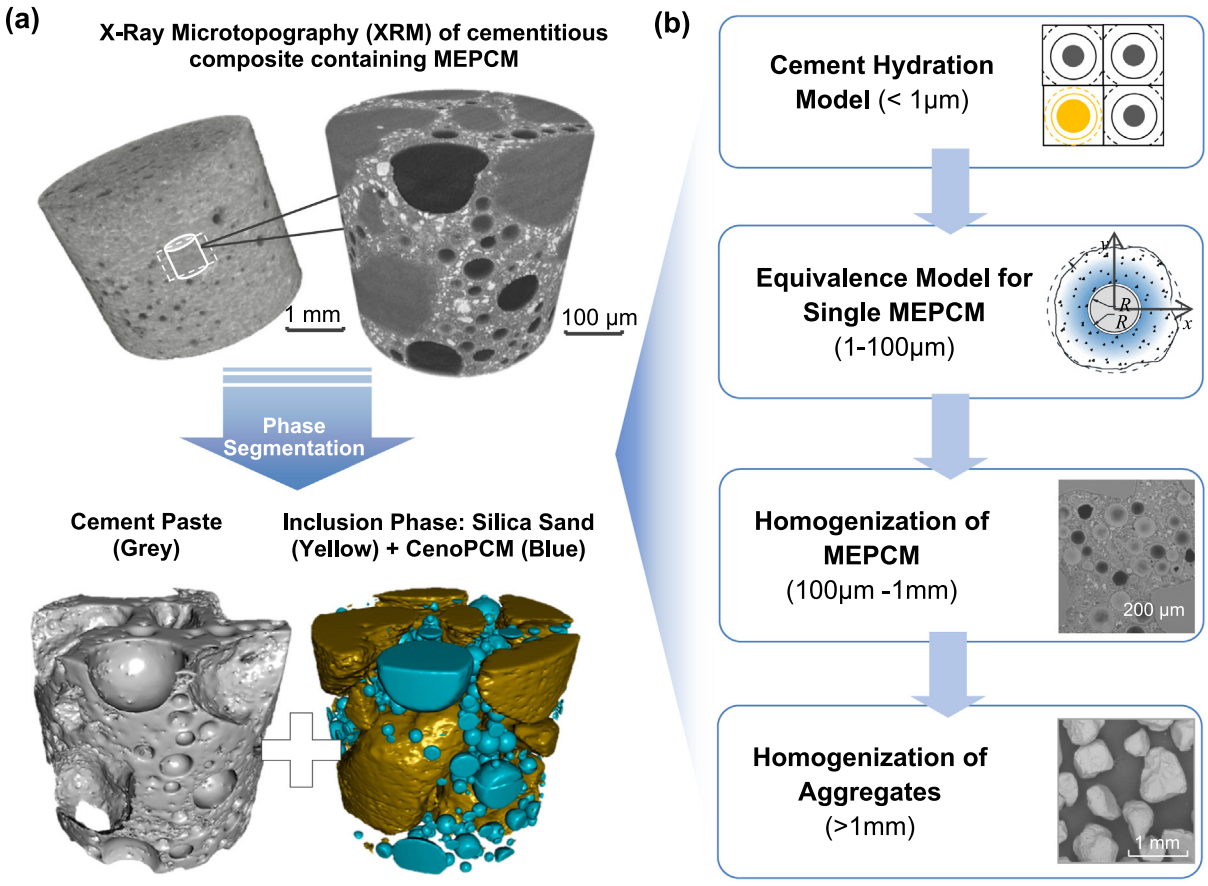

Fig. 3. The hierarchical microstructure of cementitious composite materials: (a) X-ray micro-tomography (XRM) and 3D reconstruction of the cementitious matrix and the inclusion phases; and (b) models at different scales considered.

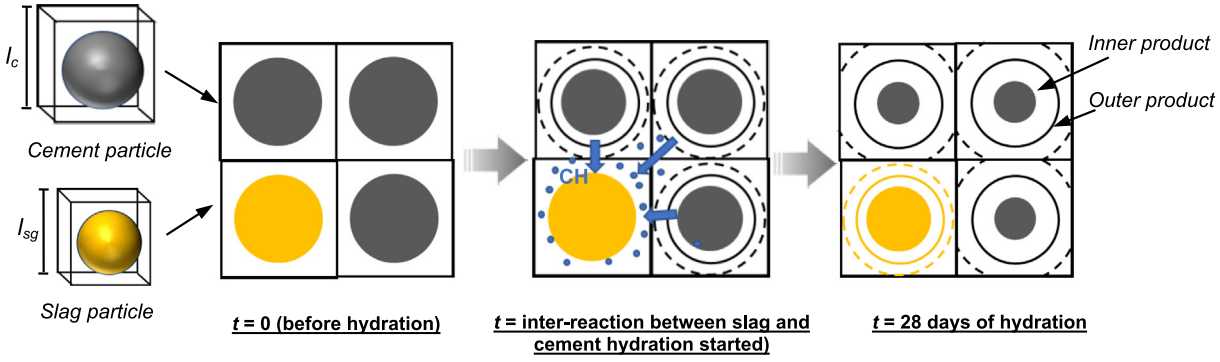

Fig. 4. Schematic hydration and microstructure development of slag-blended cement matrix [32].

$$\alpha_c = \sum_{k=1}^{4} \alpha_k m_k / \sum_{k=1}^{4} m_k \tag{16}$$

where α_k is the degree of hydration of the clinker phases of cement, C_3S, C_2S, C_3A, and C_4AF, respectively; α_c is the degree of cement hydration which is calculated as the weighted average of the clinker phases; $\omega_{dc} = B_{1c}/\alpha_c^{1.5} + B_{2c}\alpha_c^3$ is the effective diffusion coefficient of capillary water through C-S-H gel with B_{1c} representing the rate of the initial shell formation and B_{2c} describes the rate of the initial shell decay; $D_{ec} = D_{ec0}\ln(1/\alpha_c)$ is the effective diffusion coefficient of water;ω_{rk} is the reaction coefficient of the boundary reaction process for the k^{th} clinker; $\upsilon = 0.25$ is the stoichiometric ratio of mass of water to mass of cement; $w_g = 0.15$ is the physically bound water in hydration products; ρ_w is the density of water; $CW_{free} = ((m_w - 0.4\alpha m_c)/m_w)^H$ is the amount of capillary water at the exterior of hydration products with m_w and m_c are the mass of water and cement respectively and $H = 1.0$ when water to cementitious binder ratio (w/c) is larger than 0.4; and $H = 2.6 - 4m_w/(m_c + m_{sg})$ with m_{sg} is the mass of the slag when w/c is less than 0.4; S_w and S_0 are the effective contact area between the surrounding capillary water and cement particles and the total area when cement hydration products progress unconstrained.

μ_{1c}, μ_{2c}, μ_{3c}, and $\mu_{4c}$are temperature sensitivity coefficients of B_{1c}, B_{2c}, ω_{rk}, and D_{ec0} respectively; and the influence of curing temperature (T) on reaction coefficients follows Arrhenius's lows as [30]:

$$B_{1c} = B_{1c20}\exp(-\mu_{1c}(1/T - 1/293)) \quad (17\text{-}1)$$

$$B_{2c} = B_{2c20}\exp(-\mu_{2c}(1/T - 1/293)) \quad (17\text{-}2)$$

$$\omega_{rk} = \omega_{rk20}\exp(-\mu_{3c}(1/T - 1/293)) \quad (17\text{-}3)$$

$$D_{ec0} = D_{ec20}\exp(-\mu_{4c}(1/T - 1/293)) \quad (17\text{-}4)$$

where B_{1c20}, B_{2c20}, ω_{rk20}, and D_{ec20} are the values of B_{1c}, B_{2c}, ω_{rk}, and D_{ec0} at 20 °C respectively. The coefficients of Eqs. (15)–(17) are provided in Tables 1 and 2 respectively, and the parametersS_w can be calculated using Equation in reference [31].

On the other hand, the reaction of slag particles can be represented by [29]:

$$\frac{d\alpha_{sg}}{dt} = \frac{m_{CH}(t)}{m_{sg}}\frac{m_{cap}}{m_w}\frac{3\rho_w}{\upsilon_{sg} r_{sg0}\rho_{sg}} \frac{1}{\left(\frac{1}{\omega_{dsg}} - \frac{r_{sg0}}{D_{esg}}\right) + \frac{r_{sg0}}{D_{esg}}\left(1-\alpha_{sg}\right)^{(-1/3)} + \frac{1}{\omega_{rsg}}\left(1-\alpha_{sg}\right)^{(-2/3)}} \quad (18)$$

where α_{sg} is the degree of slag reaction, $m_{CH}(t)$ is the mass of the calcium hydroxide (CH), m_{cap} is the mass of capillary water, $\upsilon_{sg} = 0.25 - 0.1m_{sg}/(m_{sg} + m_c)$ is the stoichiometric ratio of the mass of CH to slag, r_{sg0} is the radius of the slag particle, ρ_{sg} is the density of slag, $\omega_{dsg} = B_{1sg}/\alpha_{sg}^{1.5} + B_{2sg}\alpha_{sg}^3$ is the reaction rate coefficient in the initial domain period with B_{1sg} and B_{2sg} are reaction coefficients, $D_{esg} = D_{esg0}\ln(1/\alpha_{sg})$ is the initial diffusion coefficient, and ω_{rsg} is the reaction rate coefficient of slag. μ_{1sg}, μ_{2sg}, μ_{3sg}, and μ_{4sg} are temperature sensitivity coefficients of B_{1sg}, B_{2sg}, ω_{rsg}, and D_{esg0} respectively, which take the same equation form as Eq. (17). The coefficients used in the slag reaction model Eq. (18) are listed in Table 3.

The inter-reaction between cement hydration and slag reaction depends on the amount of calcium hydroxide (CH) and capillary water left in the hydrating cement-slag system. The mass of CH in the cement-slag binder is calculated as:

$$m_{CH}(t) = RCH_{CE} \times m_c\alpha_c - \upsilon_{sg}\alpha_{sg}m_{sg} \quad (19)$$

where RCH_{CE} is the mass of CH produced from unit mass of cement hydration.

The mass of chemically bound water, m_{cbm}, and capillary water, m_{cap}, can be estimated as:

$$m_{cbm} = \upsilon m_c\alpha_c + 0.3\alpha_{sg}m_{sg} \quad (20)$$

$$m_{cap} = m_w - 0.4\alpha_c m_c - 0.45\alpha_{sg}m_{sg} \quad (21)$$

The mass of calcium silicate hydrate (C-S-H) in hardened cement can be estimated as:

$$m_{C-S-H}(t) = 3.71q_{s,c}m_c\alpha_c + 3.04q_{s,sg}\alpha_{sg}m_{sg} \quad (22)$$

where 3.71 and 3.04 are the mass ratio between the molar mass of C-S-H produced from the cement hydration and mass reaction and the mass of the oxide SiO_2 in the C-S-H respectively; $q_{s,c}$ and $q_{s,sg}$ are the weight fraction of SiO_2 in cement and slag respectively. The chemical composition of OPC Type I/II and slag are listed in Table 4 from which $q_{s,c}$ and $q_{s,sg}$ can be estimated.

With the kinetic slag-blended cement hydration model, the volume fractions of various constituents in the hydrated cement-slag matrix are calculated as:

$$\phi_{unhy,c} = \frac{m_c}{\rho_c}(1-\alpha_c) \quad (23\text{-}1)$$

$$\phi_{unhy,sg} = \frac{m_{sg}}{\rho_{sg}}(1-\alpha_{sg}) \quad (23\text{-}2)$$

$$\phi_{C-S-H} = \frac{m_{C-S-H}(t)}{\rho_{C-S-H}} \quad (23\text{-}3)$$

$$\phi_{cap} = m_{cap} + 0.0625m_c\alpha_c + 0.1\alpha_{sg}m_{sg} \quad (23\text{-}4)$$

$$\phi_{other} = 1 - \phi_{unhy} - \phi_{C-S-H} - \phi_{cap} \quad (23\text{-}5)$$

where ϕ_{unhy}, ϕ_{C-S-H}, ϕ_{cap}, and ϕ_{other} are the volume fraction of unhydrated slag-blended cement composite, C-S-H, capillary pores, and other hydration products. The elastic and thermal properties of each constituent phase are presented in Table 5. Compared with exterior C-S-H, the interior C-S-H has a larger elastic modulus and thermal conductivity because it is more dense [34].

2.2.3. Modeling of the functional inclusions

For inclusions with a hollow or core–shell configuration, such as the MEPCMs considered in this study, it can be equivalented as a solid particle having the same dimension with equivalent elastic and thermal properties, see Fig. 5. The equivalent elastic properties can be established through Eshelby's strain energy equivalence [36], and the equivalent bulk modulus of the inclusion, K_I^{eq}, is obtained as [37]:

$$K_I^{eq} = K_{shell} + \frac{(K_{core} - K_{shell})\delta}{1 + (1-\delta)[(K_{core} - K_{shell})/(K_{shell} + 4/3G_{shell})]} \quad (24)$$

where $\delta = (r_1/r_2)^3$ is the volumetric ratio of the core in a core–shell particle where r_1 is the inner radius and r_2 is the outer radius (see Fig. 5); K_{shell}, G_{shell}, and K_{core}, G_{core} are the bulk and shear moduli of the shell and core materials, respectively.

The equivalent shear modulus of a core–shell particle,G_I^{eq}, is obtained by solving:

$$A_1\left(\frac{G_I^{eq}}{G_{shell}}\right)^2 + A_2\left(\frac{G_I^{eq}}{G_{shell}}\right) + A_3 = 0 \quad (25)$$

where coefficients A_1, A_2, and A_3 are the functions of the core/shell material elastic properties and the volumetric ratio of the core δ. The formulations of A_1, A_2, and A_3 can be found in a previous paper of the authors [27].

The equivalent thermal conductivity of core–shell particle is [38]:

$$\chi_I^{eq} = \frac{2(1-\delta)\chi_{shell} + (1+2\delta)\chi_{core}}{(2+\delta)\chi_{shell} + (1-\delta)\chi_{core}}\chi_{shell} \quad (26)$$

where $\chi_{core}$and $\chi_{shell}$are the thermal conductivities of the core and shell, respectively.

A spherical inclusion with its interface transition zone (ITZ) can be treated as a composite system [39,40] and its equivalent property may be obtained by applying the Mori-Tanaka method in a differential scheme:

$$\frac{dX_{I,ITZ}^{eq}(r)}{dr} = -\frac{3}{r}\frac{\left(X_{I,ITZ}^{eq}(r) - X_{ITZ}(r)\right)}{\Gamma_{dil}^X} \quad (27)$$

Table 1
Coefficients of the cement hydration model [29]

B_{1c20} = 8.1 × 10^{-9} (cm/h)	D_{e20} = 8.6 × 10^{-10} (cm/h)
B_{2c20} = 0.02 (cm/h)	μ_{1c} = 1000 (K)
ω_{rC_3S20} = 9.0 × 10^{-6} (cm/h)	μ_{2c} = 1000 (K)
ω_{rC_2S20} = 2.7 × 10^{-7} (cm/h)	μ_{3c} = 5400 (K)
ω_{rC_3A20} = 1.4 × 10^{-6} (cm/h)	μ_{4c} = 7500 (K)
ω_{rC_4AF20} = 6.8 × 10^{-8} (cm/h)	

Table 2
Mineral components of OPC Type I [33]

	Mineral compositions					Blaine
	C_3S	C_2S	C_3A	C_4AF	$C\bar{S}_2H$	
	(mass%)	(mass%)	(mass%)	(mass%)	(mass%)	(cm^2/g)
OPC	60.0	11.0	10.0	8.0	2.5	3280

Table 3
Coefficient of the slag reaction model [29]

B_{1sg20}	B_{2sg20}	ω_{rsg20}	D_{esg20}	μ_{1sg}	μ_{2sg}	μ_{3sg}	μ_{4sg}
(cm/h)	(cm/h)	(cm/h)	(cm/h)	(K)	(K)	(K)	(K)
8.9×10^{-9}	0.1	1.0×10^{-5}	1.9×10^{-9}	1000	1000	5000	7000

Table 4
Chemical composition of cement.

	Chemical composition (mass%)						Blaine
	SiO_2	Al_2O_3	Fe_2O_3	CaO	MgO	SO_3	(cm^2/g)
Cement	19.2	5.16	2.47	62.6	3.48	3.57	3280
Slag	35.1	11.4	1.7	33.9	13.8	0.0	4000

Table 5
Thermal and elastic properties of hydration products and unhydrated materials of cement-slag mixture [35]

	C-S-H (interior)	C-S-H (exterior)	CH	other	air	unhy,c	unhy,sg
E (GPa)	30.3	24.2	37.2	24.2	1.0×10^{-4}	90.3	60.0
ν (-)	0.2	0.2	0.31	0.2	0.0	0.3	0.25
χ(W/mK)	0.96	0.9	1.32	0.9	0.026	3.4	3.0
ρ(kg/m^3)	2400	2300	2240	2300	12.25	3200	3200

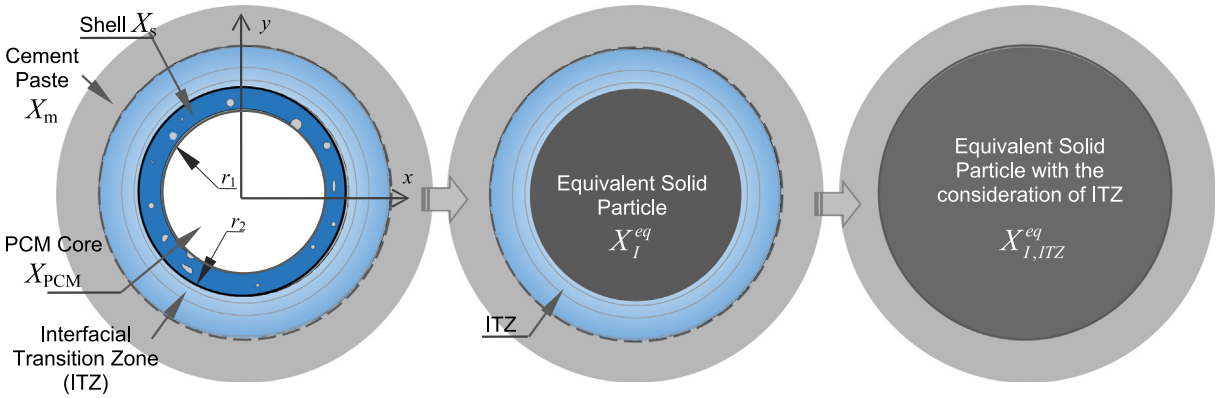

Fig. 5. Equivalence of a core–shell MEPCM particle and its around interface transition zone (ITZ) to a solid particle.

where Γ_{dil}^{X} is the dilute concentration factor,$X_{I,ITZ}^{eq}$is the equivalent properties – i.e., the elastic properties (bulk modulus and shear modulus) and thermal conductivity, of the core–shell particle (CSP) inclusion including the interface layer.

$$X_{ITZ}(r) = X_m + (X_{ITZ,\min} - X_m)(r/r_2)^{-\psi} \text{ with } r_2 < r < r_2 + r_{ITZ} \quad (28)$$

where $X_{ITZ,\min}$ is the minimum value across the ITZ region located at the particle boundary. The power exponent $\psi = \left|\frac{1}{\ln(1+r_{ITZ}/r)} \ln\left(\frac{0.02X_m}{X_m - X_{ITZ,\min}}\right)\right|$ with r_{ITZ} is the thickness of the interface layer.

2.2.4. Homogenization

The elastic properties and thermal conductivity of the cement-composite materials are obtained through the homogenization of cement paste, aggregates, and the functional inclusions using the Mori-Tanaka model [41]. For cement paste, it is treated as a composite where the matrix is the C-S-H gel, and the inclusions are other hydration products, unhydrated clinkers/slag and pores. For cementitious composites, the obtained homogenized cement paste is used as the matrix and particles like MEPCM and sand are used as inclusions. The elastic properties the effective elastic tensor, $\bar{\mathbf{C}}$, of a composite system containing n classes inclusions (the i^{th}) may be estimated as:

$$\bar{\mathbf{C}} = \mathbf{C}_m + \sum_{i=1}^{n} \phi_i (\mathbf{C}_{I,i} - \mathbf{C}_m) \Gamma^{\mathrm{C}}_{(MT),i} \tag{29}$$

where ϕ_i is the volume fraction of the i^{th} inclusion; $\mathbf{C}_{I,i}$ and $\mathbf{C}_m$are the elastic tensors of the i^{th} class inclusion and the matrix, respectively; and $\Gamma^{\mathrm{C}}_{(MT),i}$is the Mori-Tanaka strain concentration tensor of the i^{th} inclusion:

$$\Gamma^{\mathrm{C}}_{(MT),i} = \left[\phi_i \mathbf{I} + \phi_m \left(\Gamma^{\mathrm{C}}_{dil,i} \right)^{-1} + \sum_{j=1}^{N} \phi_j \Gamma^{\mathrm{C}}_{dil,j} \left(\Gamma^{\mathrm{C}}_{dil,i} \right)^{-1} \right]^{-1}, \; j \neq i \tag{30}$$

where $\mathbf{I}$ is a fourth order identity tensor, ϕ_m is the volume fraction of the matrix, and $\Gamma^{\mathrm{C}}_{dil,i}$is the strain concentration tensor of the i^{th} inclusion under dilute scheme [41]:

$$\Gamma^{\mathrm{C}}_{dil,i} = \left[\mathbf{I} + \mathbf{S}^{\mathrm{C}}_m \mathbf{C}_m^{-1} (\mathbf{C}_{I,i} - \mathbf{C}_m) \right]^{-1} \tag{31}$$

$\mathbf{S}^{\mathrm{C}}_m$ is the Eshelby's tensor, which can be found in [42].

Similarly, for the effective thermal conductivity tensor,$\bar{\chi}$:

$$\bar{\chi} = \chi_m + \sum_{i=1}^{N} \phi_i \left(\chi_{I,i} - \chi_m \right) \Gamma^{\chi}_{(MT),i} \tag{32}$$

where $\chi_{I,i}$, χ_m are the thermal conductivity tensor of the i^{th} class inclusion and matrix respectively, and $\Gamma^{\chi}_{(MT),i}$ is the temperature gradient concentration tensor [43].

The effective volumetric heat of fusion (*VHF*) can be simply obtained by [44]:

$$VHF = \phi_{pcm} \rho_{pcm} L_{pcm} \tag{33}$$

where L_{pcm} is the latent heat of fusion of PCM.

2.2.5. Material cost and carbon footprint

For a unit volume (1 m^3) of the composite cementitious material, its material cost is simply calculated as the summation of the constituent material cost:

$$Cost = \sum m_h \times Cost_h \tag{34}$$

where m_h and $Cost_h$ are the mass and unit cost of the constituent materials with h = cement, slag, water, silica sand, and phase change material (PCM). Given the volume fraction of cement-slag binder (ϕ_b), volume fraction of sand (ϕ_s), volume fraction of PCM (ϕ_{pcm}), water to cementitious binder ratio (w/c), and slag replacement ratio (rr_{sg}), then the mass of each constituent can be calculated from Eqs. (35-1)–(35-5):

$$\phi_b = \frac{m_w}{\rho_w} + \frac{m_c}{\rho_c} + \frac{m_{sg}}{\rho_{sg}} \tag{35-1}$$

$$\phi_s = \frac{m_s}{\rho_s} \tag{35-2}$$

$$\phi_{pcm} = \frac{m_{pcm}}{\rho_{pcm}} \tag{35-3}$$

$$w_b = \frac{m_w}{m_c + m_{sg}} \tag{35-4}$$

$$rr_{sg} = \frac{m_{sg}}{m_c + m_{sg}} \tag{35-5}$$

Similarly, the CO_2 footprint (CO_2) can be calculated as:

$$CO_2 = \sum \left(m_h \times CO_{2(h)} \right) \tag{36}$$

where $CO_{2(h)}$ is the embodied carbon of the h^{th} material per unit mass during material production phase. It is noted that the CO_2 emission during other processes such as transportation is not considered in this study for simplicity.

3. Multi-objective optimization and decision making

3.1. Multi-objective feasibility enhanced particle swarm optimization algorithm

The multi-objective optimization (MOO) problem for the mixture design of cementitious material containing MEPCMs can be formulated as the minimization of the objective functions:

$$\min F(\mathbf{x}) = \min[-f_1(\mathbf{x}), -f_2(\mathbf{x}), -f_3(\mathbf{x}), f_4(\mathbf{x}), f_5(\mathbf{x})]^T \tag{37}$$

where $\mathbf{x} = [w_b, rr_{sg}, \phi_m, \phi_s, \phi_{pcm}]^T$ is the vector of design variables. The MOO problem is subject the constraints given in Eqs. (6)–(11).

The Pareto-optimal set can be obtained by the multi-objective feasibility enhanced particle swarm optimization (MOFEPSO) algorithm [19]. The MOFEPSO algorithm starts with the initialization of particle swarm with random positions ($\mathbf{p}$) and velocities ($\mathbf{v}$). Then, the MOFEPSO separates particles into feasible particles and infeasible particles, where infeasible particles violate at least one constraint. For feasible particles, the objective functions are evaluated and the non-dominated results are stored in global optimal set $\mathbf{B}$ and personal optimal set $\mathbf{D}_\tau$. For both feasible particles and non-feasible particles, their velocities at time $t + 1$ are updated as:

$$v_{\tau,\eta}(t+1) = \xi v_{\tau,\eta}(t) + C_1 z_{1,\eta} \left(p^{\Lambda}_{\eta} - p_{\tau,\eta}(t) \right) + C_2 z_{2,\eta} \left(p^{\Omega}_{\tau,\eta} - p_{\tau,\eta}(t) \right) \tag{38}$$

$$v_{\tau,\eta}(t+1) = \Xi_{a,\eta} \left[\xi v_{\tau,\eta}(t) + C_1 z_{1,\eta} \left(p^{\Lambda}_{\eta} - p_{\tau,\eta}(t) \right) \right] \tag{39}$$

where, ξ is the inertia factor, C_1 and C_2 are the social (global) and cognitive (personal) acceleration coefficient respectively, $z_{1,\eta} \in [0,1]$ and $z_{2,\eta} \in [0,1]$ are uniformly distributed random numbers of the decision variable η, p^{Λ}_{η} and $p^{\Omega}_{\tau,\eta}$ are the randomly selected global and personal best from global and personal non-dominated sets for feasible particle τ. For infeasible particle, the global guide is selected randomly from the set of current positions of particles that does not violate the constraint satisfied previously. Moreover, the velocities of feasible and infeasible particles are updated differently. For feasible particle, the velocity at time $t + 1$ depends on the inertia factor, global best and personal best, see Eq. (38). For non-feasible particle, it only relies on the inertia factor and global best, see Eq. (39). A sensitivity coefficient $\Xi_{a,\eta}$ [19] is used to guide infeasible particle moves to the most sensitive direction, where each direction represents one decision variable. Thus, the new candidate position of both feasible and infeasible particles is calculated as:

$$p_{\tau,\eta}(t+1) = p_{\tau,\eta}(t) + v_{\tau,\eta}(t+1) \tag{40}$$

At step $t + 1$, new candidate position may violate some constraints, i.e., decision variable limits and constrain functions, which were already satisfied at step t. To avoid particle moving to a worse location, the new candidate particle is enforced with decision variable limits and virtual boundary limits to ensure those constraints which satisfied at step t are still maintained at step $t + 1$. For detailed information of sensitivity coefficient and enforcing decision variable limits and virtual boundary limits, please refer to the work of Hasanoglu and Dolen [19].

3.2. Multi-criteria decision making

While the Pareto-optimal set provides critical information about potential design options, it still needs a multi-criteria

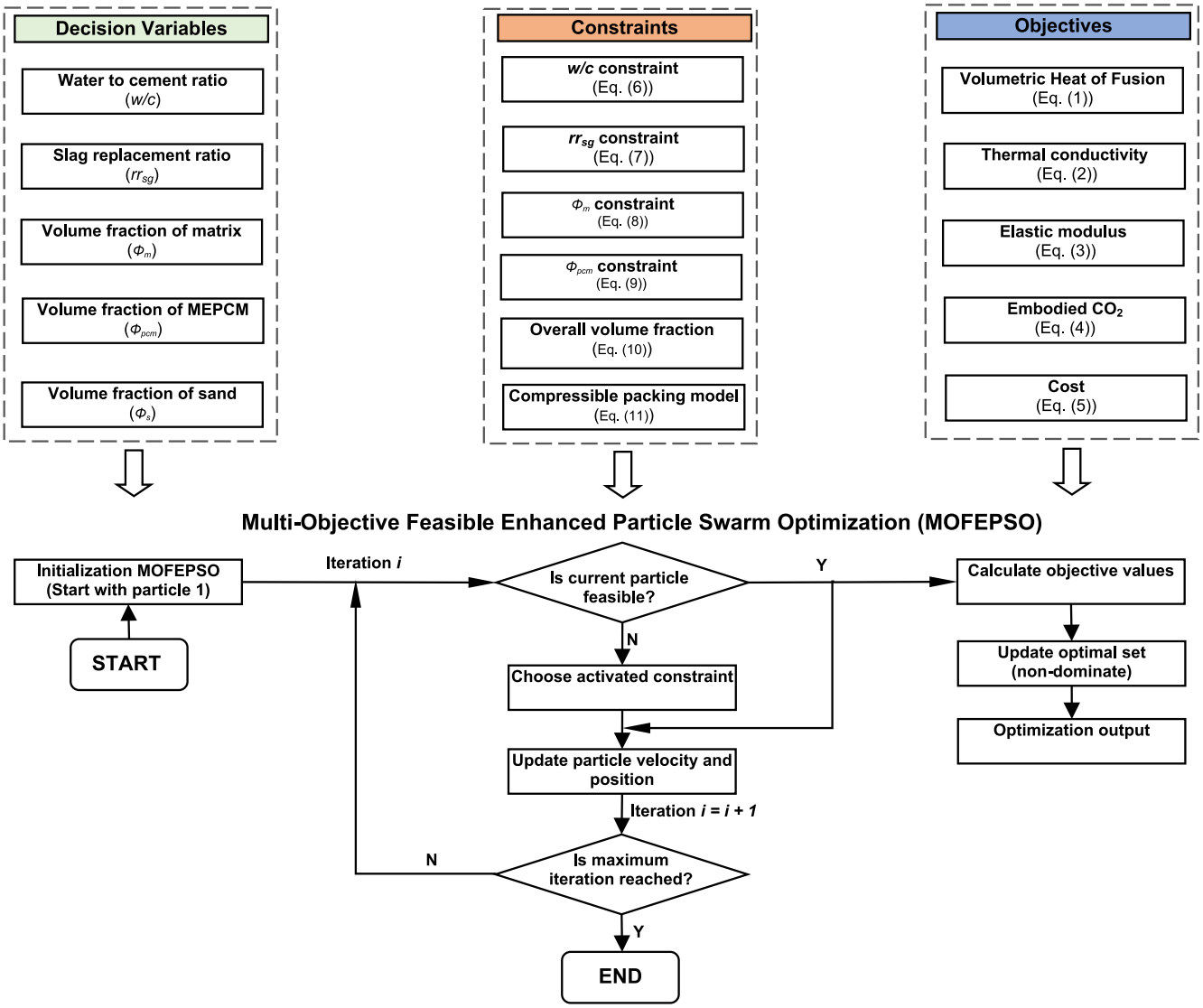

Fig. 6. Flow chart showing the optimization process.

decision-making model to assist the final decision making. In this paper, the Technique for Order Preference by Similarity to Ideal Solution (TOPSIS) [45] is used for selecting the optimal mixture candidate from the Pareto-optimal set. TOPSIS selects an alternative that is closest to the positive ideal point and furthest from the negative idea point. In the Pareto-optimal set, the positive ideal point, ε_{η}^{+}, is defined as, e.g., the mixture design has the maximum value for preferable function value (or minimum value for non-preferable function value) and the negative ideal point, ε_{η}^{-}, is defined as the one has the minimum value for preferable function value (or maximum value for non-preferable function value). For the design of a concrete mixture, the positive ideal points of VHF_{eff}, χ_{eff}, and E_{eff} are their maximum values in the mixture design optimal set; whilst the positive ideal points of *Cost*, and CO_2 are their corresponding minimum values; and vice versa for the negative ideal points. Then, the distance from the positive ideal point (σ_o^+) and the distance from the negative ideal point (σ_o^-) for the o^{th} point in the Pareto-optimal set can be calculated as:

$$\sigma_o^+ = \sqrt{\sum_{u=1}^{U} \left(\varepsilon_{ou} - \varepsilon_u^+\right)^2} \tag{41}$$

$$\sigma_o^- = \sqrt{\sum_{u=1}^{U} \left(\varepsilon_{ou} - \varepsilon_u^-\right)^2} \tag{42}$$

where $\varepsilon_{ou} = \Upsilon_{ou} w_u$ $(o = 1, \cdots, O;\ u = 1, \cdots, U)$ and $\Upsilon_{ou} = \frac{\kappa_{ou}}{\sqrt{\kappa_{ou}^2 + \cdots + \kappa_{Ou}^2}}$ is the normalized value for the u^{th} criteria (totally U) of the o^{th} point (totally O) with κ_{ou} the corresponding objective value, and w_u is the weight of the u^{th} criteria which can be either assigned subjectively by experts or calculated objectively through mathematical equations such as the entropy method [46]. For functional cementitious composites, different mixture design scenarios can be specified and the weights of the criteria can be assigned accordingly [47], which will be further illustrated in the following sections.Then, the final mixture design is ranked and selected by the closeness coefficient, CC_o^+, of each alternative:

$$CC_o^+ = \frac{\sigma_o^-}{\left(\sigma_o^- + \sigma_o^+\right)} \quad o = 1, 2, \cdots, O \tag{43}$$

The optimization steps are summarized in the flowchart shown in Fig. 6.

Table 6
Test matrix and mix proportions (by weight, kg of materials /m^3 of concrete).

Mix ID	MEPCM Vol (%)	MEPCM	Water	Cement	Silica Sand	Quartz Powder	Air Content
Control	0.0	0	244	762	1270	62	0.010
Micronal-036	3.6	36	243	759	1170	56	0.016
Micronal-072	7.2	71	242	756	1069	52	0.021
Micronal-108	10.8	106	241	753	969	47	0.027
Micronal-144	14.4	141	240	751	872	42	0.031
Micronal-179	17.9	176	239	748	773	38	0.045
Micronal-214	21.4	210	238	743	674	33	0.066
CenoPCM-029	2.9	48	243	760	1170	59	0.023
CenoPCM-058	5.8	97	245	766	1083	54	0.025
CenoPCM-086	8.6	145	245	767	987	49	0.033
CenoPCM-116	11.6	194	246	770	894	45	0.038
CenoPCM-145	14.5	244	247	772	798	40	0.046
CenoPCM-174	17.4	293	248	774	701	35	0.054
CenoPCM-203	20.3	341	246	769	578	29	0.077

4. Experimental study

The physics-based models for predicting the thermal conductivity and elastic modulus of functional cementitious composites are validated through two sets of experimental data with two types of MEPCMs, i.e., polymer encapsulated paraffin phase change material (PolyPCM) and the fly ash cenosphere encapsulated PCM (CenoPCM) recently developed by the authors [1]. The main purpose of the experimental mixture design is to validate and calibrate the physics-based models with different volume fractions of MEPCMs.The functional cementitious material was made using ASTM C150 compliant Type I/II ordinary Portland cement (OPC), Ottawa silica sand, grounded quartz/silica flour, and MEPCMs. The commercially available PolyPCM – Micronal® was used in the experimental study. The cost information of PolyPCM was estimated based on a US Department of Energy report [48].

The experimental mixtures have a water to cement ratio (w/c) of 0.32. For cementitious composites containing PolyPCM (Micronal®) and CenoPCM, equivalent volume of sand and quartz powder (fine aggregate) was substituted by the MEPCMs. Details of the mixture design is provided in Table 6, and the experimental setup and testing results were described in a previous work by the authors [49].

Inclusion and interfacial transition zone (ITZ) properties and the modeling parameters are listed in Tables 7 and 8. The shell thickness of PolyPCM (Micronal®) and CenoPCM are 1 μm and 8 μm, respectively. The ITZ thickness is selected to be a function of D_{50} (cumulative 50% point of particle diameter) where larger particle has a relatively thicker ITZ. The minimum ITZ properties are calibrated as a function of cement matrix where CenoPCM has relatively higher values compared with PolyPCM mainly due to the pozzolanic reaction of silica and CH in the ITZ interface [49].

Fig. 7 (a) and (b) compare the predicted effective thermal conductivity and elastic modulus with experimental values. The results show that the physics-based models established in this study can represent the experiment values very well. In Fig. 7 (a), the experiments were conducted both below and above the phase change temperature (T_{pc}) of the MPCMs at age 28 days and temperature shows negligible effect on the measured thermal conductivities as expected. The elastic modulus was measured at age 7 days and 28 days to examine the effect of curing time and relatively small differences were observed, see Fig. 7 (b).

5. Case studies

As shown in Section 2, the physics-based models for predicting the thermal conductivity (χ), elastic modulus (E), CO_2 footprint (CO_2), volumetric heat of fusion (VHF), and cost ($Cost$) are functions of water to cementitious binder ratio (w/c), slag replacement ratio (rr_{sg}), and the volume fractions of binder, sand, and functional additives (e.g., MEPCMs).

5.1. Optimal mixture design of MEPCMs-cementitious composites

In the mixture design of cementitious composites containing MEPCMs, five objectives (mixture design decision variables), i.e., thermal conductivity (χ), elastic modulus (E), carbon footprint (CO_2), volumetric heat of fusion (VHF), and cost, are used to find the optimal mixture design as functions of five design variables, i.e., water to cementitious binder ratio (w/c), slag replacement ratio (rr_{sg}), volume fraction of cement paste, and the volume fractions of sand and MPCMs. The models calibrated with experimental data are used for obtaining the optimal mixture design of cementitious composites containing MEPCMs (i.e., PolyPCM and CenoPCM). The Pareto-optimal set is for the mixture design obtained by the MOFEPSO.

After obtaining the Pareto-optimal set for the mixture design, decision making charts are created through paired comparisons of the mixture design decision variables according to the scores obtained by TOPSIS ranking method, where a weights vector needs to be defined. The TOPSIS score is calculated for each option in the optimal mixture design set. Eight different weight vectors are designed to represent the decision scenarios of 'strength', 'green', 'thermal - heat storage (T-HS)', 'thermal – conductivity (T-C)', 'cost', 'balanced', 'structural-energy (S-ENG)', and 'structural-environment (S-ENV)' [47]. For each scenario, its weights vector includes the weights coming from four main categories, i.e., mechanical properties, thermal properties, CO_2, and cost, with the summation of the main categories weights equals to one. In each main category, it may be further divided into several sub-categories – e.g., the thermal properties can be divided into 'volumetric heat of fusion' and 'thermal conductivity'. The weights of the sub-categories in each main category represents their related importance. The 'strength' scenario is used for design cases where compressive strength is the main consideration in the functional cementitious composites design. A similar scenario design approach is applied to designing 'green', 'T-HS', 'T-C', and 'cost'. Moreover, a 'balanced' scenario and two strength constrained scenarios (with minimum strength of 17.2 MPa 'S-ENG' and 'S-ENV') were also considered. The 'balanced' scenario was designed to consider a balanced performance among mechanical, thermal properties, cost, and environment impact (CO_2); while the 'S-ENG' and 'S-ENV' scenarios were designed to consider cases where the minimum strength was required for structural use [20] with considering energy performance and environmental performance

Table 7
Inclusion and ITZ properties.

Inclusion type	D_{50}	t_s	t_{ITZ}	$\chi_{ITZ,min}$	$E_{ITZ,min}$
	(um)	(um)	(um)	(W/mK)	(GPa)
Sand	640	–	$0.05D_{50}$	$0.1\chi_m$	$0.1E_m$
PolyPCM (Micronal®)	20	1	$0.5D_{50}$	$0.1\chi_m$	$0.01E_m$
CenoPCM	90	8	$0.15D_{50}$	$0.6\chi_m$	$0.6E_m$

Table 8
Physical, thermal, mechanical, economic, and environmental properties of constituents in the studied cementitious materials containing MEPCMs.

Material	Cement	Slag	Sand	CenoPCM*		PolyPCM**		Water
				Core	Shell	Core	Shell	
E (GPa)	90.3	60.0	72.0	0.0557	96.0	0.0557	2.1	–
v (-)	0.3	0.25	0.17	0.499	0.21	0.499	0.37	–
χ(W/mK)	3.4	3.0	4.0	0.25	1.60	0.25	0.20	0.604
ρ(kg/m^3)	3200	2800	2650	1250		982.4		1000
L (kJ/kg)	–	–	–	75.69		90.31		–
Cost ($/kg)	0.1235	0.09	0.09	1.7		5.7		0.005
CO_2*** (kg/kg)	1.017	0.091	0.003	0.033		0.208		0

* Cost of CenoPCM is estimated by reaching a storage capacity cost of 50 $/kWh which can be achieved through combining innovative microencapsulation technology of cenosphere and relative low cost fatty acid PCM.
** Cost of polymer encapsulated paraffin wax phase change material (PolyPCM) is estimated by using the data presented in[48].
*** CO_2 footprints of cement and slag are estimated by the online GreenConcrete LCA tool [50] and obtained from reference [51]. Meanwhile, the CO_2 footprints of MEPCM materials are adopted from [52].

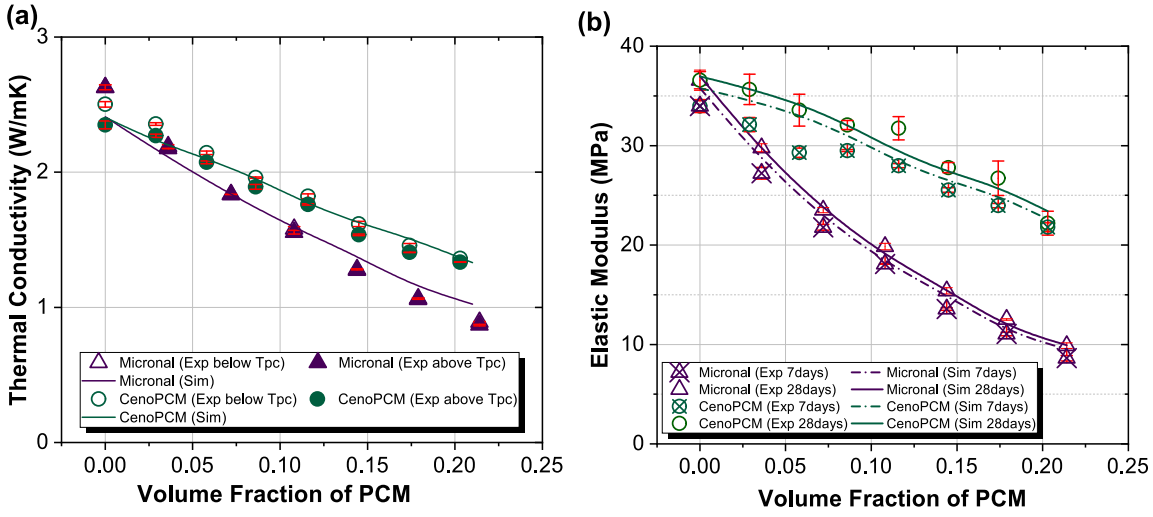

Fig. 7. Model validations for functional cementitious materials containing Micronal® and CenoPCM: (a) thermal conductivity; (b) elastic modulus at the age of 7 days and 28 days.

Table 9
Weights of designed scenarios for optimal mixture design decision making.

Categories	F*	Scenario							
		Strength	Green	T-HS	T-C	Cost	Balanced	S-ENG**	S-ENV
Mechanical properties	S	**65%**	**20%**	**20%**	**20%**	**10%**	**40%**	–	–
Compressive strength	*S1*	*80%*	*80%*	*40%*	*40%*	*80%*	*60%*	–	–
Modulus of elasticity	*S2*	*20%*	*20%*	*60%*	*60%*	*20%*	*40%*	–	–
Thermal properties	T	**5%**	**10%**	**50%**	**50%**	**30%**	**10%**	**60%**	**25%**
Volumetric heat of fusion	*T1*	*40%*	*80%*	*80%*	*50%*	*80%*	*40%*	*80%*	*80%*
Thermal conductivity	*T2*	*60%*	*20%*	*20%*	*50%*	*20%*	*60%*	*20%*	*20%*
CO_2	L	**10%**	**50%**	**10%**	**10%**	**10%**	**20%**	**20%**	**50%**
Cost	C	**20%**	**20%**	**20%**	**20%**	**50%**	**30%**	**20%**	**25%**

* F: Factor of category.
** Minimum strength of 17.2 MPa was used as constraints for 'S-ENG' and 'S-ENV'.

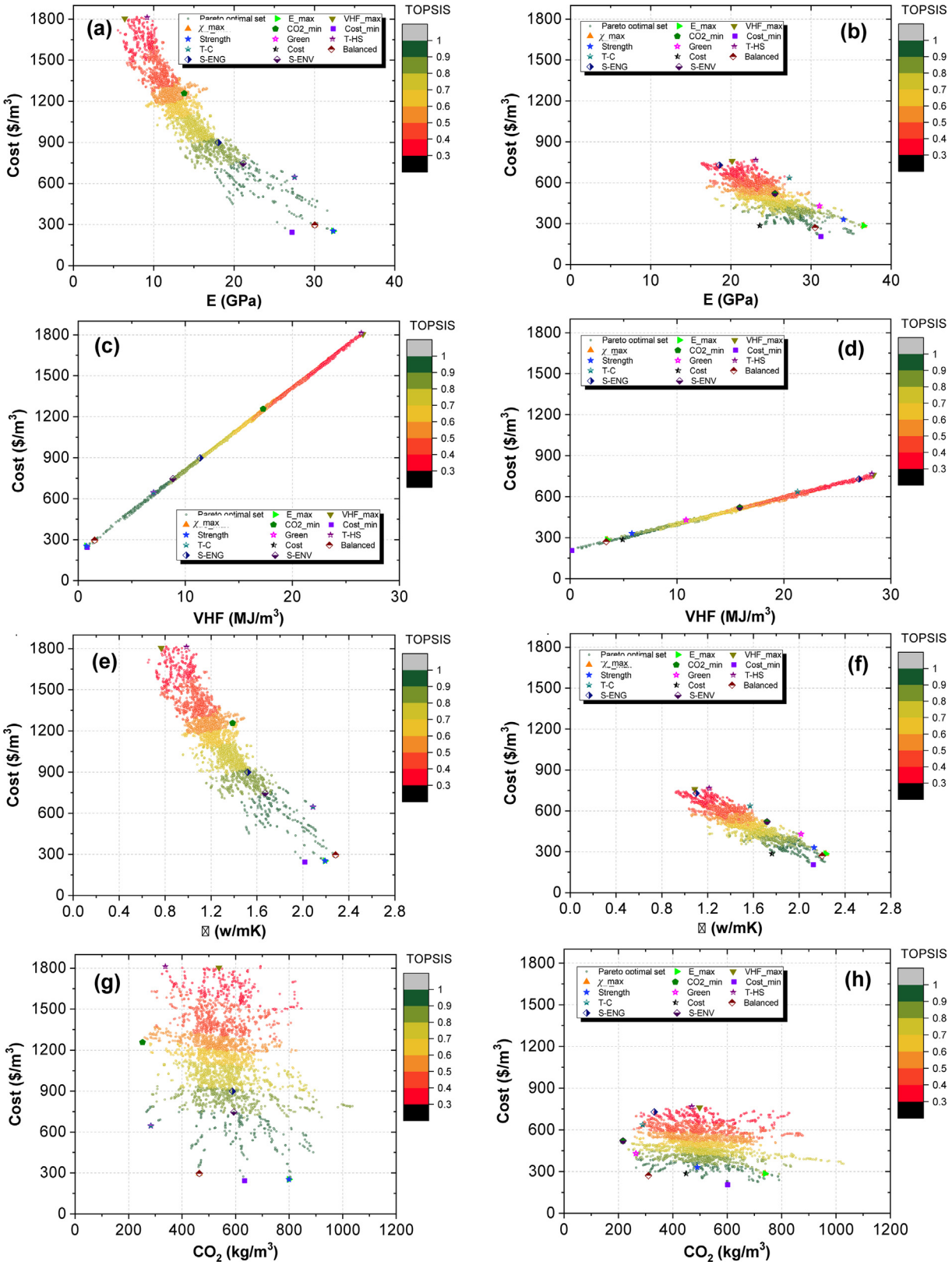

Fig. 8. Mixture design decision making charts of cementitious composites containing MEPCMs for the Cost scenario: (a), (b) elastic modulus (E); (c), (d) volumetric heat of fusion (VHF); (e), (f) thermal conductivity (χ); and (g), (h) CO_2 footprint for PolyPCM and CenoPCM respectively.

optimization. The weights in each main category and sub-category depend on the selected scenario. For example, the 'T-HS' and 'T-C' scenarios are designed to emphasize the importance of heat storage and thermal conductivity of functional cementitious composites respectively, see Table 9. 'S-ENG' and 'S-ENV' scenarios did not assign weights to mechanical properties since strength and elastic modulus were implemented as constraints in the multi-criteria decision making (MCDM) process. The compressive strength, f_c, is estimated by ACI 318 [20] based on the elastic modulus and density of concrete.

Fig. 8 presents the mixture design decision making charts of cementitious composites containing MEPCMs for the cost scenario, where the color bar indicates the TOPSIS scores for the obtained Pareto-optimal mixture design set. The points of maximum thermal conductivity (χ_max), maximum E (E_max), maximum VHF (VHF_max), minimum CO_2 (CO_2_min), and minimum cost (Cost_min) refer to single-objective optimization cases when each of the performance criteria is the sole objective of the optimal mixture design problem. Using the TOPSIS decision making method, mixture designs of different scenarios can be obtained. The ideal points that have the highest TOPSIS scores for the eight scenarios are also plotted in the mixture design decision making charts. It is clear that the optimal mixture design determined by the TOPSIS method is a compromise between different design objectives. For example, the TOPSIS decision-making method for the "T-HS" scenario leads to optimal mixture designs with elastic modulus (E) of 9.18 and 23.11 GPa for cementitious composites containing PolyPCM and CenoPCM, respectively. The design mixtures of the single-objective and TOPSIS decision making method are presented in Tables 10 and 11 and plotted in Fig. 9. The parallel plot of Fig. 9 indicates the existence of conflicts between the objectives of χ and E and the objectives of VHF and cost as they are dominated by the amounts of MEPCMs. Generally, the increase of MEPCMs leads to higher VHF and cost and lower χ and E. χ and E are also influenced by the amount of sand and binder (cement and slag), and the water to binder ratio. However, the CO_2 footprint is dictated by the amount of cement since it has the largest CO_2 footprint. The lower amount of cement and the higher amount slag replacement ratio can effectively reduce the CO_2 footprint. The structural performance requirement generally leads to the reduction of the amount of PolyPCM in cementitious composites while has little influence on the amount of CenoPCM due to its high strength, see Fig. 10 (a).

The mixture design decision-making charts (see Fig. 8) show that the cementitious composites containing the CenoPCM, which uses a rigid inorganic shell (fly ash cenosphere) as capsules, is more suitable for applications that have strength requirement (e.g., building envelope panels and floor slabs) due to its better mechanical performance, higher thermal conductivity, and lower cost compared with cementitious composites containing polymer encapsulated PCMs (PolyPCM). This is also reflected from the plotted distributions of the obtained optimal mixture design set, see Fig. 10. The compressive strength of cementitious composites containing CenoPCM is distributed in the range 30 – 50 MPa; whereas cementitious composites containing PolyPCM is distributed in the range 5–20 MPa. Meanwhile, the cost of cementitious composites containing CenoPCM ranges from 300 to 750 $/m^3 based on its estimated costs, which is promising for building applications.

The decision-making charts developed herein can assist users/-material designers to select and determine mixture designs of functional cementitious composite materials in the early stage design. For example, if a user is interested in designing a cementitious composite containing MEPCM with a cost lower than 1000 $/m^3. Their achievable VHF, elastic modulus, and thermal conductivity can be found from design charts similar to that presented in Fig. 8. The mixture design decision making charts for the scenarios of "strength", "green", "T-HS", "T-C", "Balanced", "S-ENG" and "S-ENV" are not all plotted to be concise. It is noted that the mixture design of MEPCMs cementitious composites also relies on the application space. For example, for building envelope applications the cost-benefit can be further quantified by building energy simulations with consideration of energy saving and the benefit from peak load shedding. In this research, only material related properties are considered in the decision making.

5.2. CO_2 and cost savings of cementitious composites containing CenoPCM

Fig. 11 presents specific CO_2 and cost as functions of volumetric heat of fusion (VHF). The specific CO_2 and cost are calculated by normalize the CO_2 footprint and cost obtained by the optimization with their corresponding compressive strength. As indicated by the fitted relationships, the specific CO_2 and cost of cementitious composites containing CenoPCM shows a linear relationship whilst its PolyPCM counterpart has an exponential relationship. While they have similar CO_2 footprint (see Fig. 10 (c)), the cementitious composites containing CeonPCM has much lower specific CO_2 because its higher strength. Interestingly, the specific CO_2 of cementitious composites containing CenoPCM tends to be a constant which indicates that reduction of CO_2 footprint due to increasing the amount of CenoPCM is almost equal to the reduction of the compressive strength. On the other hand, the specific CO_2 of cementitious composites containing PolyPCM increases almost exponentially with the increase of VHF which is mainly caused by its low compressive strength (see Fig. 11 (a)). The specific cost increases with the add-

Table 10
Characteristic mixture designs of cementitious composites containing PolyPCM.

Mixture	cement	slag	ϕ_{pcm}	sand	w/c	E	VHF	χ	CO_2	Cost
	(kg/m^3)	(kg/m^3)	(-)	(kg/m^3)	(-)	(GPa)	(MJ/m^3)	(W/mK)	(kg/m^3)	($/m^3)
E_max	776.6	46.9	0.009	1114.4	0.37	32.34	0.78	2.19	799.6	253.2
VHF_max	441.6	208.5	0.300	454.3	0.43	6.40	26.59	0.77	537.8	1805.2
TC_max	442.1	67.5	0.017	1486.9	0.50	30.05	1.54	2.28	464.4	295.8
CO_2_min	188.7	131.0	0.195	1372.5	0.49	13.79	17.28	1.39	252.4	1257.3
Cost_min	605.7	135.2	0.009	1062.6	0.47	27.22	0.84	2.02	633.8	242.8
Strength	776.6	46.9	0.009	1114.4	0.37	32.34	0.78	2.19	799.6	253.2
Green	235.9	223.4	0.079	1573.3	0.36	27.53	7.04	2.09	283.2	645.8
T-HS	248.6	154.9	0.298	984.8	0.40	9.18	26.44	0.99	337.7	1812.1
T-C	235.9	223.4	0.079	1573.3	0.36	27.53	7.04	2.09	283.2	645.8
Cost	442.1	67.5	0.017	1486.9	0.50	30.05	1.54	2.28	464.4	295.8
Balanced	442.1	67.5	0.017	1486.9	0.50	30.05	1.54	2.28	464.4	295.8
S-ENG	537.1	102.6	0.128	1077.6	0.38	18.04	11.39	1.52	588.2	898.3
S-ENV	543.1	161.2	0.100	1082.1	0.35	21.14	8.85	1.67	593.2	746.3

Table 11
Characteristic mixture designs of cementitious composites containing CenoPCM.

Mixture	cement	slag	ϕ_{pcm}	sand	w/c	E	VHF	χ	CO_2	Cost
	(kg/m^3)	(kg/m^3)	(-)	(kg/m^3)	(-)	(GPa)	(MJ/m^3)	(W/mK)	(kg/m^3)	($/m^3$)
E_max	716.3	53.7	0.037	1230.4	0.30	36.57	3.46	2.23	739.2	285.1
VHF_max	459.9	148.8	0.300	512.1	0.37	20.18	28.38	1.09	498.6	760.8
TC_max	716.3	53.7	0.037	1230.4	0.30	36.57	3.46	2.23	739.2	285.1
CO_2_min	188.7	131.0	0.168	1372.5	0.49	25.50	15.87	1.72	216.9	521.0
Cost_min	567.6	227.6	0.002	1115.0	0.39	31.25	0.16	2.12	601.7	205.3
Strength	452.5	248.2	0.061	1237.5	0.31	34.07	5.78	2.13	490.0	330.8
Green	230.1	217.9	0.115	1430.1	0.36	31.05	10.84	2.02	264.4	430.0
T-HS	439.4	52.5	0.298	789.3	0.33	23.11	28.22	1.21	469.7	766.9
T-C	256.4	145.8	0.225	1191.9	0.32	27.32	21.27	1.57	289.5	636.5
Cost	412.5	264.1	0.052	972.7	0.49	23.62	4.92	1.76	449.5	284.9
Balanced	280.2	205.1	0.036	1479.4	0.47	30.50	3.38	2.20	310.2	271.5
S-ENG	288.8	236.1	0.285	607.8	0.44	18.57	27.01	1.10	332.1	728.8
S-ENV	188.7	131.0	0.168	1,372.5	0.49	25.50	15.87	1.72	216.9	521.0

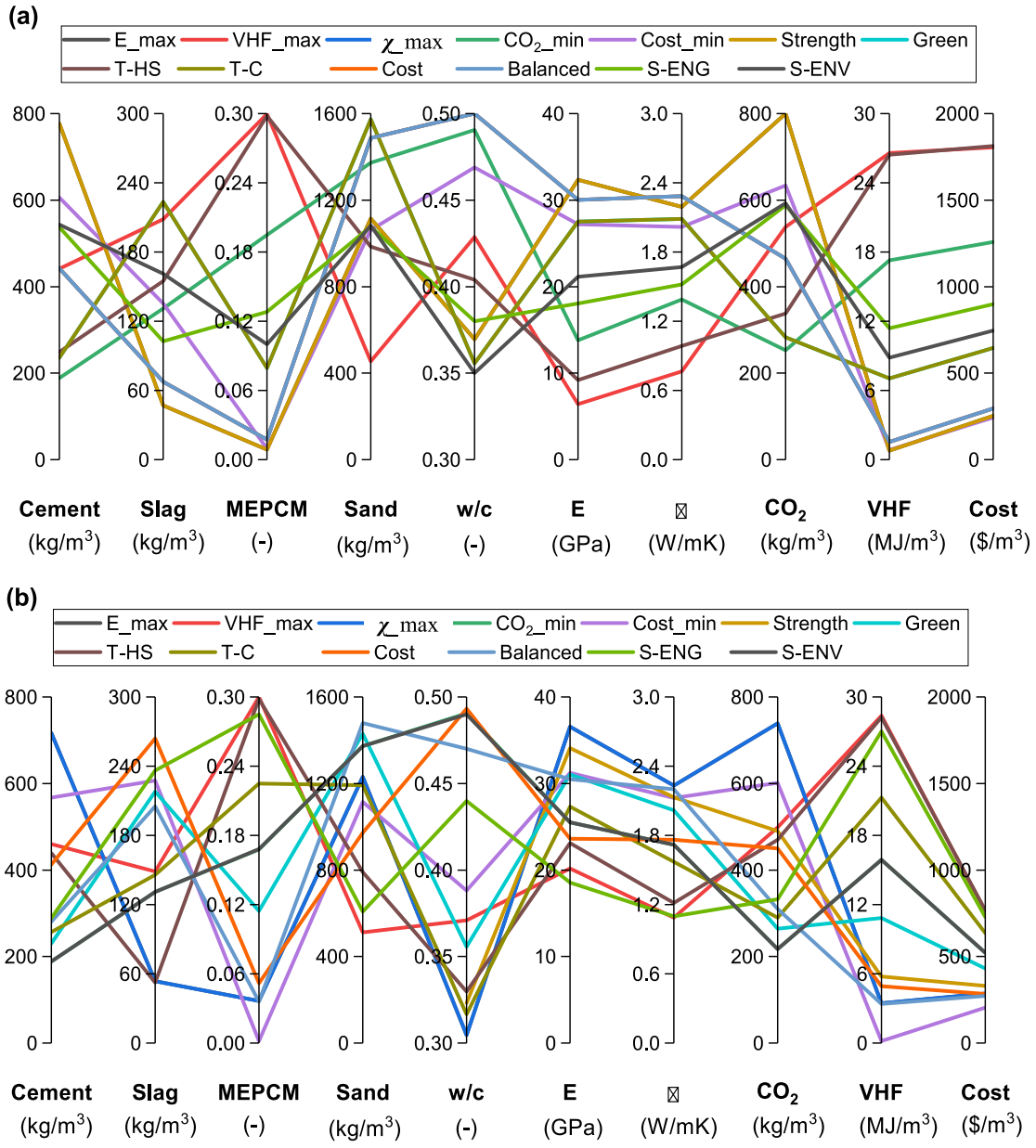

Fig. 9. Parallel plots for characteristic mixture designs of: (a) cementitious composites containing PolyPCM; and (b) cementitious composites containing CenoPCM.

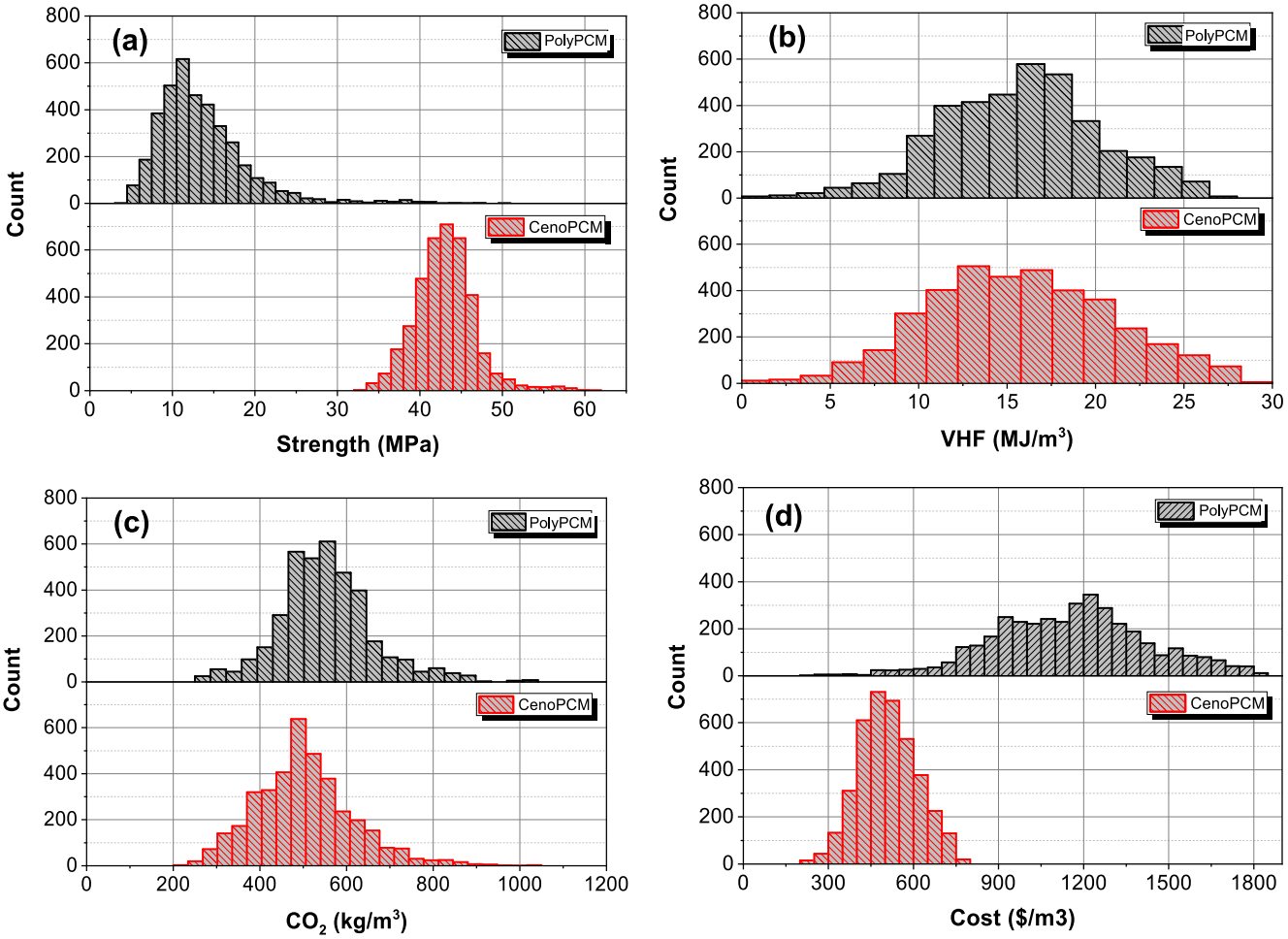

Fig. 10. Distributions of obtained optimal mixture design set for cement composites containing PolyPCM and CenoPCM: (a) strength; (b) volumetric heat of fusion (VHF); (c) CO_2 footprint; and (d) cost.

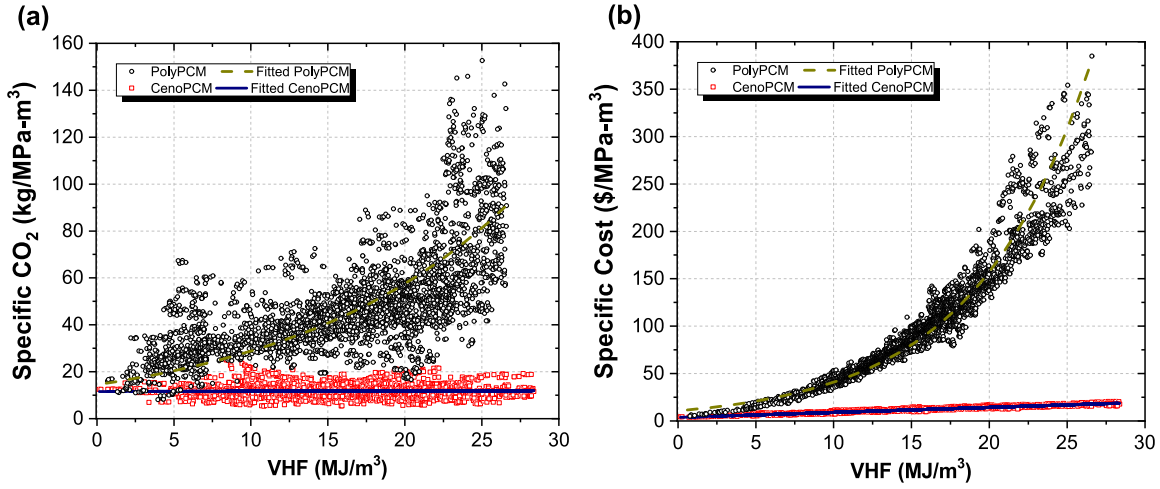

Fig. 11. CO_2 footprint and cost of cementitious composites containing PolyPCM and CenoPCM normalized by compressive strength: (a) specific CO_2; and (b) specific cost.

ing of both PolyPCM and CenoPCM, see Fig. 11 (b), due to the higher price of MEPCMs compared with other constituents of MEPCMs cementitious composites. Similarly, the specific cost of cementitious composites containing CenoPCM is much lower than its PolyPCM counterpart.

The CO_2 saving of utilizing CenoPCM cementitious composites is obvious for strength specified design applications. Assume a nonstructural component such as building envelope have a minimum VHF of 15 MJ/m^3, then the specific CO_2 saving is about 29.0 kg/m^3. In other word, it saves about 71% of specific CO_2 when

adopting CenoPCM instead of PolyPCM. It is worthwhile to mention that the decision on PCM type also depends on its market availability, cost and properties of the PCM such as melting temperature. A detailed discussion of the selection of PCM type is outside the range of this study, more information and discussion can be found in references [2,53].

6. Conclusion remarks

This paper presents a physics-guided, multi-objective optimization procedure for optimal mixture design of cementitious composites containing functional fillers (i.e., microencapsulated phase change materials, or MEPCMs). The mixture design procedure developed herein combines physics-based models with multi-objective optimization and multi-criteria decision making (MCDM) methods to aid the mixture design decision-making given a specific user defined preference (i.e., mechanical performance, cost, sustainability, or functionality). The multi-objective feasible enhanced particle swarm optimization (MOFEPSO) algorithm and the technique for preference by similarity to an ideal solution (TOPSIS) algorithm are used to find the optimal mixture design sets and aid the decision-making. Functional cementitious composites with two types of MEPCMs – i.e., a polymer microencapsulated PCM (PolyPCM) and the rigid shell cenosphere microencapsulated PCM (CenoPCM), are compared in the case study. The results show that:

- Generally, the addition of MEPCMs leads to the reduction of both thermal conductivity and elastic modulus, while cement composites with the newly developed CenoPCM has greatly improved mechanical performance and a much lower cost compared with those with polymer microencapsulated PCM.
- The mixture design decision making charts allow mechanical, thermal, environmental, and economic properties to be evaluated concurrently, which enable users to quickly find potential optimal mixture designs. Moreover, the different scenarios in the TOPSIS decision making method allows the mixture design process to be tailored for specific applications.
- The specific CO_2 footprint and cost results show obvious savings by using CenoPCM in comparison with PolyPCM in concrete applications.

Future research efforts can be directed to the following two aspects:

- Establishing the relationship between compressive strength and mixture design variables through data-driven metamodels (with sufficient data).
- Introducing more comprehensive energy performance (cost-saving) indicators by coupling, e.g., building energy simulations, in the analysis.

Declaration of Competing Interest

The authors declare that they have no known competing financial interests or personal relationships that could have appeared to influence the work reported in this paper.

Acknowledgements

This research is partially sponsored by the US Department of Energy (DE-EE-0008677) and National Science Foundation (NSF CMMI-1954517). The funding supports from DOE and NSF are greatly appreciated.

Data Availability

The raw/processed data required to reproduce these findings cannot be shared at this time due to technical or time limitations. The data is available upon request.

References

[1] F. Liu, J. Wang, X. Qian, Integrating phase change materials into concrete through microencapsulation using cenospheres, Cem. Concr. Compos. 80 (2017) 317–325, https://doi.org/10.1016/j.cemconcomp.2017.04.001.
[2] S. Drissi, T. Ling, K. Hung, A. Eddhahak, A review of microencapsulated and composite phase change materials: Alteration of strength and thermal properties of cement-based materials, Renew. Sustain. Energy Rev. 110 (2019) 467–484, https://doi.org/10.1016/j.rser.2019.04.072.
[3] F. de Larrard, T. Sedran, Optimization of Ultra-High-Performance Concrete by The Use of A Packing Model, Cem. Concr. Res. 24 (1994) 997–1009.
[4] Y. Xie, B. Liu, J. Yin, S. Zhou, Optimum mix parameters of high-strength self-compacting concrete with ultrapulverized fly ash, Cem. Concr. Res. 32 (2002) 477–480.
[5] K.A. Soudki, E.F. El-Salakawy, N.B. Elkum, Full Factorial Optimization of Concrete Mix Design for Hot Climates, J. Mater. Civ. Eng. 13 (2001) 427–433.
[6] S. Hınıslıoğlu, O.Ü. Bayrak, Optimization of early flexural strength of pavement concrete with silica fume and fly ash by the Taguchi method, Civ. Eng. Environ. Syst. 21 (2004) 79–90, https://doi.org/10.1080/10286600410001684562.
[7] A. Oztas, A. Baykasoglu, H. Ozbebek, Investigating mix proportions of high strength self compacting concrete by using Taguchi method, Constr. Build. Mater. 23 (2009) 694–702, https://doi.org/10.1016/j.conbuildmat.2008.02.014.
[8] P. Suttaphakdee, N. Dulsang, N. Lorwanishpaisarn, P. Kasemsiri, Optimizing mix proportion and properties of lightweight concrete incorporated phase change material paraffin / recycled concrete block composite, Constr. Build. Mater. 127 (2016) 475–483, https://doi.org/10.1016/j.conbuildmat.2016.10.037.
[9] N. Li, C. Shi, Z. Zhang, D. Zhu, H. Hwang, Y. Zhu, A mixture proportioning method for the development of performance-based alkali-activated slag-based concrete, Cem. Concr. Compos. 93 (2018) 163–174, https://doi.org/10.1016/j.cemconcomp.2018.07.009.
[10] D. Jiao, C. Shi, Q. Yuan, X. An, Y. Liu, Mixture design of concrete using simplex centroid design method, Cem. Concr. Compos. 89 (2018) 76–88, https://doi.org/10.1016/j.cemconcomp.2018.03.001.
[11] Z. Li, D. Lu, X. Gao, Multi-objective optimization of gap-graded cement paste blended with supplementary cementitious materials using response surface methodology, Constr. Build. Mater. 248 (2020), https://doi.org/10.1016/j.conbuildmat.2020.118552 118552.
[12] Q. Zhang, X. Feng, X. Chen, K. Lu, Mix design for recycled aggregate pervious concrete based on response surface methodology, Constr. Build. Mater. 259 (2020), https://doi.org/10.1016/j.conbuildmat.2020.119776.
[13] M.A. Derousseau, J.R. Kasprzyk, W.V. Srubar III, Computational design optimization of concrete mixtures: A review, Cem. Concr. Res. 109 (2018) 42–53, https://doi.org/10.1016/j.cemconres.2018.04.007.
[14] J. Zhang, Y. Huang, Y. Wang, G. Ma, Multi-objective optimization of concrete mixture proportions using machine learning and metaheuristic algorithms, Constr. Build. Mater. 253 (2020), https://doi.org/10.1016/j.conbuildmat.2020.119208 119208.
[15] B.A. Young, A. Hall, L. Pilon, P. Gupta, G. Sant, Can the compressive strength of concrete be estimated from knowledge of the mixture proportions?: New insights from statistical analysis and machine learning methods, Cem. Concr. Res. 115 (2019) 379–388, https://doi.org/10.1016/j.cemconres.2018.09.006.
[16] A. Baykasoglu, A. Öztas, E. Ozbay, Prediction and multi-objective optimization of high-strength concrete parameters via soft computing approaches, Expert Syst. Appl. 36 (2009) 6145–6155, https://doi.org/10.1016/j.eswa.2008.07.017.
[17] S. Kwon, X. Wang, Optimization of the Mixture Design of Low-CO2 High-Strength Concrete Containing Silica Fume, Adv. Civ. Eng. 2019 (2019) 1–9.
[18] E. Mohammadi, A. Behnood, Estimating the optimal mix design of silica fume concrete using biogeography-based programming, Cem. Concr. Compos. 96 (2019) 95–105, https://doi.org/10.1016/j.cemconcomp.2018.11.005.
[19] M.S. Hasanoglu, M. Dolen, Multi-objective feasibility enhanced particle swarm optimization, Eng. Optim. 0273 (2018), https://doi.org/10.1080/0305215X.2018.1431232.
[20] ACI Committee 318. ACI 318-19: Building Code Requirements for Structural Concrete and Commentary. American Concrete Institute; 2019.
[21] H. Lee, X. Wang, L. Zhang, K. Koh, Analysis of the Optimum Usage of Slag for the Compressive Strength of Concrete, Materials (Basel) 1213–29 (2015), https://doi.org/10.3390/ma8031213.
[22] F. de Larrard, Concrete mixture proportioning: a scientific approach, London and New York: E & FN SPON, 1999.
[23] G. Roquier, The 4-parameter Compressible Packing Model (CPM) including a new theory about wall effect and loosening effect for spheres, Powder Technol. 302 (2016) 247–253, https://doi.org/10.1016/j.powtec.2016.08.031.
[24] S. Das, M. Aguayo, S.D. Rajan, G. Sant, N. Neithalath, Microstructure-guided numerical simulations to predict the thermal performance of a hierarchical

cement-based composite material, Cem. Concr. Compos. 87 (2018) 20–28, https://doi.org/10.1016/j.cemconcomp.2017.12.003.
[25] E. Ghossein, M. Lévesque, A comprehensive validation of analytical homogenization models: The case of ellipsoidal particles reinforced composites, Mech. Mater. 75 (2014) 135–150, https://doi.org/10.1016/j.mechmat.2014.03.014.
[26] E.J. Garboczi, D.P. Bentz, Analytical formulas for interfacial transition zone properties, Adv. Cem. Based Mater. 6 (1997) 99–108.
[27] Z. Shen, H. Zhou, Predicting effective thermal and elastic properties of cementitious composites containing polydispersed hollow and core-shell micro-particles, Cem. Concr. Compos. 105 (2020), https://doi.org/10.1016/j.cemconcomp.2019.103439 103439.
[28] X.Q. Feng, S.W. Yu, Estimate of effective elastic moduli with microcrack interaction effects, Theor. Appl. Fract. Mech. 34 (2000) 225–233.
[29] L. Han-seung, X. Wang, Evaluation of compressive strength development and carbonation depth of high volume slag-blended concrete, Constr. Build. Mater. 124 (2016) 45–54, https://doi.org/10.1016/j.conbuildmat.2016.07.070.
[30] F. Tomosawa, Development of a kinetic model for hydration of cement. Proceeding 10th Int, Congr. Chem. Cem. Gothenburg, Sweden (1997) 1–8.
[31] K. Park, T. Noguchi, J. Plawsky, Modeling of hydration reactions using neural networks to predict the average properties of cement paste, Cem. Concr. Res. 35 (2005) 1676–1684, https://doi.org/10.1016/j.cemconres.2004.08.004.
[32] G. Ye, B.K. Van, Simulation of connectivity of capillary porosity in hardening cement-based systems made of blended materials, Heron 54 (2009) 163–184.
[33] W. Chen, H.J.H. Brouwers, The hydration of slag, part 2: reaction models for blended cement, J. Mater. Sci. (2007) 444–464, https://doi.org/10.1007/s10853-006-0874-1.
[34] G. Constantinides, F.J. Ulm, The effect of two types of C-S-H on the elasticity of cement-based materials: Results from nanoindentation and micromechanical modeling, Cem. Concr. Res. 34 (2004) 67–80, https://doi.org/10.1016/S0008-8846(03)00230-8.
[35] M.J. Qomi Abdolhosseini, F. Ulm, R.J. Pellenq, Physical Origins of Thermal Properties of Cement Paste, Phys. Rev. Appl 064010 (2015) 1–17, https://doi.org/10.1103/PhysRevApplied.3.064010.
[36] J.D. Eshelby, The Continuum Theory of Lattice Defects, Solid State Phys. – Adv. Res. Appl. 3 (1956) 79–144, https://doi.org/10.1016/S0081-1947(08)60132-0.
[37] R.M. Christensen, K.H. Lo, Solutions for Effective Shear Properties in Three Phase Sphere and Cylinder Models, J. Mech. Phys. Solids 27 (1979) 315–330.
[38] Z. Jia, Z. Wang, D. Hwang, L. Wang, Prediction of the Effective Thermal Conductivity of Hollow Sphere Foams, ACS Appl. Energy Mater. 1 (2018) 1146–1157, https://doi.org/10.1021/acsaem.7b00264.
[39] L. Shen, J.J. Li, Effective elastic moduli of composites reinforced by particle or fiber with an inhomogeneous interphase, Int. J. Solids Struct. 40 (2003) 1393–1409, https://doi.org/10.1016/S0020-7683(02)00659-5.
[40] L. Shen, J. Li, Homogenization of a fibre/sphere with an inhomogeneous interphase for the effective elastic moduli of composites, Proc. R Soc. A Math. Phys. Eng. Sci. 461 (2005) 1475–1504, https://doi.org/10.1098/rspa.2005.1447.
[41] B. Klusemann, B. Svendsen, Homogenization methods formulti-phase elastic composites: Comparisons and benchmarks, Tech. Mech. 30 (2010) 374–386.
[42] J.D. Eshelby, The Determination of the Elastic Field of an Ellipsoidal Inclusion, and Related Problems, Proc. R Soc. London Ser. A Matchematical Phys. Sci 241 (1957) 376–396.
[43] J. Stránský, J. Vorel, J. Zeman, M. Šejnoha, Mori-tanaka based estimates of effective thermal conductivity of various engineering materials, Micromachines 2 (2011) 129–149, https://doi.org/10.3390/mi2020129.
[44] A.M. Thiele, G. Sant, L. Pilon, Diurnal thermal analysis of microencapsulated PCM-concrete composite walls, Energy Convers Manag 93 (2015) 215–227, https://doi.org/10.1016/j.enconman.2014.12.078.
[45] C. Hwang, Y. Lai, T. Liu, A New Approach for Multiple Objective Decision Making, Comput. Oper. Res. 20 (1993) 889–899.
[46] M. Alemi-ardakani, A.S. Milani, S. Yannacopoulos, G. Shokouhi, On the effect of subjective, objective and combinative weighting in multiple criteria decision making: A case study on impact optimization of composites, Expert Syst. Appl. 46 (2016) 426–438, https://doi.org/10.1016/j.eswa.2015.11.003.
[47] R. Kurda, B.J. De, J.D. Silvestre, CONCRETop - A multi-criteria decision method for concrete optimization, Environ. Impact Assess. Rev. 74 (2019) 73–85, https://doi.org/10.1016/j.eiar.2018.10.006.
[48] J. Kosny, N. Shukla, A. Fallahi, Cost Analysis of Simple Phase Change Material-Enhanced Building Envelopes in Southern U.S, Climates (2013).
[49] A.L. Brooks, Y. Fang, Z. Shen, J. Wang, H. Zhou, Enabling high-strength cementitious composite for thermal energy storage through fly-ash cenosphere encapsulated phase change materials, Cem. Concr. Compos. (2020), https://doi.org/10.1016/j.cemconcomp.2021.104033.
[50] UC Berkeley. GreenConcrete LCA Tool n.d. http://greenconcrete.berkeley.edu/ (accessed October 12, 2020).
[51] K. Yang, Y. Jung, M. Cho, S. Tae, Effect of supplementary cementitious materials on reduction of CO2 emissions from concrete, J. Clean Prod. 103 (2015) 774–783, https://doi.org/10.1016/j.jclepro.2014.03.018.
[52] K. Menou, A. Castell, M.M. Farid, D. Boer, L.F. Cabeza, Life Cycle Assessment of experimental cubicles including PCM manufactured from natural resources (esters): A theoretical study, Renew Energy 51 (2013) 398–403, https://doi.org/10.1016/j.renene.2012.10.010.
[53] C. Barreneche, M.E. Navarro, L.F. Cabeza, A.I. Fernández, New database to select phase change materials: Chemical nature, properties, and applications, J. Energy Storage 3 (2015) 18–24, https://doi.org/10.1016/j.est.2015.08.003.